Forests **2015**, *6*, 4245-4294; doi:10.3390/f6114245

OPEN ACCESS

forests

ISSN 1999-4907

www.mdpi.com/journal/forests

Article

SimpleTree —An Efficient Open Source Tool to Build Tree Models from TLS Clouds

Jan Hackenberg [1,*], Heinrich Spiecker [1], Kim Calders [2,3], Mathias Disney [2,4] and Pasi Raumonen [5]

[1] Chair of Forest Growth, University of Freiburg, Tennenbacher Street 4, 79106 Freiburg, Germany; E-Mails: jan.hackenberg@iww.uni-freiburg.de (J.H.); instww@uni-freiburg.de (H.S.)

[2] Department of Geography, University College London, London WC1E 6BT, UK; E-Mails: kim.calders@npl.co.uk (K.C.); mathias.disney@ucl.ac.uk (M.D.)

[3] Earth Observation, Climate and Optical Group, National Physical Laboratory, Hampton Road, Teddington, Middlesex TW11 0LW, UK

[4] NERC National Centre for Earth Observation (NCEO), UCL Geography, Gower Street, London WC1E 6BT, UK

[5] Department of Mathematics, Tampere University of Technology, P.O. Box 553, Tampere 33101, Finland; E-Mail: pasi.raumonen@tut.fi

* Author to whom correspondence should be addressed;
E-Mail: jan.hackenberg@iww.uni-freiburg.de; Tel. : +49-761-203-8589 Fax.: +49-761-203-3740

Academic Editor: Juha Hyyppä, Xinlian Liang and Eetu Puttonen

Received: 23 July 2015 / Accepted: 10 November 2015 / Published: 23 November 2015

Abstract: An open source tool named SimpleTree, capable of modelling highly accurate cylindrical tree models from terrestrial laser scan point clouds, is presented and evaluated. All important functionalities, accessible in the software via buttons and dialogues, are described including the explanation of all necessary input parameters. The method is validated utilizing 101 point clouds of six different tree species, in the main evergreen and coniferous trees. All scanned trees have been destructively harvested to get accurate estimates of above ground biomass with which we assess the accuracy of the SimpleTree-reconstructed cylinder models. The trees were grouped into four data sets and for each one a Concordance Correlation Coefficient of at least 0.92 (0.92, 0.97, 0.92, 0.94) and an total relative error at most $\sim$ 8 % (2.42%, 3.59%, –4.59%, 8.27%) was achieved in the comparison of the model results to the ground truth data. A global statistical improvement of derived cylinder radii is presented as well as an efficient optimization approach to automatically improve user given input parameters. An additional check of the SimpleTree results is presented via comparison to the results of trees reconstructed using an alternative, published method.

Keywords: biomass; density; volume; TLS; forestry; tree; stem; branch; point cloud; open source; software

1. Introduction

Since the early 2000s Light Detection and Ranging (LiDAR) has been used to estimate forestry parameters [1–4]. Terrestrial Laser Scanning (TLS) typically utilizes LiDAR systems mounted on a tripod, from which multiple million points can be collected within minutes. Tree and plot models derived from those TLS clouds commonly became more and more accurate with improved automation in the model computation [5–7].

In general, forestry applications are more concerned with timber form and quality and less with the size and arrangement of smaller woody components. However, for estimating above ground biomass (AGB, *i.e.*, the standing mass of carbon), gap fraction, crown shape and other more general ecological properties, higher order branch structure and topology are important. Here we describe the development and application of a new reconstruction tool, SimpleTree, which generates such models.

The identification and accurate modelling of higher order branches is one of the key differences that may arise in the application between an approach aimed specifically at forest management as opposed to a more general approach such as that followed here. The proposed approach results in geometrical models describing the complete above-ground woody tree components in an hierarchical order. Such models can be referred to as Quantitative Structure Models (QSMs) [8–11], a convention we will follow here. QSM methods still rely on AGB measurements destructively harvested to be accurately validated [9–11].

The SimpleTree method described here produces topologically ordered cylinder parameters (size, orientation) for all branches resolved by the LiDAR data, which can be of the order of thousands of branches per tree. The described method, originally proposed in Hackenberg *et al.* [12], has been shown to demonstrate an average sub-mm fit accuracy for complete tree models. However, results in Hackenberg *et al.* [10] show that with a pure geometrical fitting approach, AGB tends to be overestimated in the thinner branches. Here, we present a statistical solution to this problem.

Estimates of tree AGB are typically hard to validate due to the difficulty of obtaining data from harvested trees. Several recently published tree modelling methods rely on AGB measurements combined with density values to be validated [9–11,13,14]. Direct measurements of the tree volume can be also done through the usage of a xylometer, but this method is reported time-consuming and error-prone [15].

Providing research results in the form of an open source software is beneficial in maintaining the relevance of the method in future years. Free software gives users freedom regarding their ability to run the program as needed. Modifications of the program can be performed on open source code. Users can help others by redistributing the software. Contributions to the community can be done by sharing adaptations and new features with others [16]. Hence the approach here has been to present the tree reconstruction software SimpleTree as an open source tool.

Tree models derived from TLS point clouds can be complex to compute: between different data sets and methods, many parameters can vary. The reflecting surface of woody components in a canopy varies substantially, both within and between species, as well as over an individual. Surface and material properties have a large impact on the reflected intensity values of the beam [17], especially if the incident angle varies [18]. Undesirable weather conditions increase the amount of noise in the point clouds [10]. Different scan modes, *i.e.*, using multiple scan locations versus scanning from a single location, can have a large impact on the accuracy of the retrieved forestry parameters [14,19,20]. Various methods utilized for co-registration of multiple scans exist, with different strengths and weaknesses [21,22]. Additionally, varying the scan resolution will also have an impact on accuracy and may require adapting reconstruction methods. In practice, these acquisition characteristics are a function of instrument performance and a trade-off against time required for data collection.

We consider it necessary to develop methods that are robust to such random effects, while knowing that robustness is likely to be a trade-off with accuracy, time, and user input/effort. Under this assumption free software with open source code seems to be an appropriate tool to develop a robust, and hence more durable approach, as adaptation can also be performed by an experienced end-user.

1.1. Related Work

Nowadays TLS methods have a wide rage in computational forestry. The majority of reconstruction approaches have proposed methods aiming for forest management purposes. Stable and robust parameters—used to predict AGB—are estimated to enable those methods to be applied to a larger scale. Efforts to transform TLS based methods into vehicle based laser scanning (VLS) methods have been reported [23,24]. Yao *et al.* [25] predict AGB on plot level utilizing the Diameter at Breast Height (DBH) as an input variable for the following allometric equation:

$$AGB = a \times DBH^b. \tag{1}$$

Stem models derived as proposed in Litkey *et al.* [26] were utilized to detect changes in the forest structure over time in Liang *et al.* [27]. Yang *et al.* [28] retrieve DBH, height, crown width and crown height as well as a digital elevation model and a canopy height model from plot level scans. Kankare *et al.* [14] calculate 83 geometrical and point cloud features for 64 laboratory measured trees and reduce the number of features with lasso regression and stepwise regression. Statistical models using up to eight features as explanatory variables are used to model total AGB, stem AGB, living branch AGB and dead branch AGB. Srinivasan *et al.* [29] predict AGB change utilizing scans of different years in a similar manner, reducing the feature space of TLS derived predictors with stepwise regression to a 3D parameter space. Srinivasan *et al.* [30] analyse the accuracy of DBH, tree height and crown width estimations on plot level scans - utilizing both single and dual scan mode. A more geometrical AGB prediction method is presented in Feliciano *et al.* [31] for mangrove trees. The authors model the stem and the root system as paraboloids/torus sections and derive AGB from the total volume multiplied with a density value and a literature derived biomass expansion factor.

In Othmani *et al.* [32] the authors developed a tree species classification routine based on relief maps of the bark structure. Kretschmer *et al.* [33] detected scars in the stem surface utilized for stem quality prediction. Stem quality was also automatically classified in Kankare *et al.* [34]. Béland *et al.* [35,36] discuss the capabilities of TLS predictions of leaf area density. Voxel based methods to predict the volume of AGB components are reported as well [37,38].

1.1.1. Methods in Computational Forestry producing QSMs of the Branching Structure

QSM methods are capable of measuring the complete woody biomass volume directly. AGB can therefore be predicted in a non destructive way [10] without relying on harvested ground truth data used to train statistical models [12]. Also AGB distributions within a single tree can be modelled accurately [12].

Pfeifer *et al.* [4] present an automatic method capable of modelling the stem and branching structure of a tree. After the input cloud is partitioned into branch segments [39] for each point the normal vector is generated. From those normals initial guesses for the cylinder axes are derived. The cylinder parameters are adjusted in a least squares sense. Visual output depicts both that the resulting cylinder models are accurate but incomplete.

One reported QSM method is relying on Dijkstra's algorithm [41]. In Côté *et al.* [42] TLS points are subdivided into wood and foliage components. Then Dijkstra's algorithm is applied on the wood points to calculate a skeleton representing the stem and the major branches. To reconstruct the thinner branching structure, high occurrences of foliage are detected in voxel space. Those voxels are called attractors and are connected to the main skeleton in an iterative routine. Radii for cylinder estimations from the final skeleton are estimated from the pipe model theory [43]. Finally, foliage is added to the models. Validation to ground truth of this method was performed in Côté *et al.* [44] on basal area and total leaf area of 215 trees. The relative difference on plot level between model values and measurements was –0.01% and –0.25% respectively.

Dassot *et al.* [13] investigated point clouds of 42 trees of different species and varying size classes. With Polyworks software (Canadian Measurement-Metrology Inc., Mississauga, ON, Canada) the skeletons of those trees can be determined manually. Wood volume is afterwards calculated by using a geometric fitting procedure utilizing the skeletons. Wrongly fitted cylinders are identified visually and are manually removed from the models. A total relative error of ∼10% for the stems and ∼30% for the branches was estimated in the comparison to the ground truth data.

Eysn *et al.* [45] present another manual QSM approach. In AutoCAD [46] software 34 scan positions are processed manually for skeletonization of 120 trees with the results being merged subsequently. Cylinders are fitted automatically and outliers are removed manually. Accuracy of this method was assessed for five randomly selected trees using cloud-to-model distance analysis. This showed an average fit accuracy of sub-cm.

Belton *et al.* [47] successfully de-noised point clouds of evergreen trees automatically. Features are here extracted after performing a Principal Component Analysis (PCA) on neighbouring point coordinates. Eigenvalues and their ratios and differences serve as features. Leaf points are isolated from biomass points in feature space through a Gaussian mixture model [48]. From the points related to woody biomass horizontal slices are generated, into which ellipses are fitted. Neighbouring ellipse center points in different layers are connected to build a skeleton. The extracted skeleton is utilized in a cylinder fitting routine to build a cylindrical tree model. The authors compared the volume of an applied allometric function (34 m^3) to the volume results of the cylinder model (74 m^3) as validation.

An established tree modelling method from TLS-data is the method developed by Raumonen *et al.* [49]. This method produces a QSM of the tree [9,11], as does the SimpleTree method described here. The method [49] imports a TLS-point cloud and reconstructs the tree as a hierarchical collection of cylinders or other building blocks, as described in Åkerblom *et al.* [50]. From the resulting QSM it is possible to approximate almost any geometrical or topological attribute or distributions describing tree attributes, such as stem and branch volumes and lengths, and branch size distributions for each branching order. In Calders *et al.* [9] this QSM approach was further developed and validated on 65 tree models derived from scans of a native Eucalyptus open forest plot. Comparison to destructively harvested ground truth data revealed a total AGB overestimation of 9.68% and a Concordance Correlation Coefficient (CCC) of 0.98.

Wang *et al.* [40] skeletonize a tree cloud with a minimum distance spanning tree. After the skeleton is generated, the occluded point cloud regions with missing data are recovered. The skeleton is obtained again in a second iteration and smoothed by a Laplacian function. Radii related to skeleton lines are computed in a last step before the tree model can be enriched with leaf models. Tree models were validated with DBH field measurements ($R^2 = 0.92$).

Hackenberg *et al.* [12] developed the method which forms the basis of the SimpleTree approach capable of fitting up to 10,000 cylinders into point clouds of *Prunus avium* trees. This method was improved and implemented in SimpleTree. The clouds are derived from high resolution scans of multiple scan positions. The scans were barely affected by wind and therefore considered to be of high quality. Spheres centred on the tree skeleton are used to follow the tree's branching structure from the root to its tips. If the sphere radius is larger than the underlying cylinder radius, the sub point cloud on the sphere surface will represent circular cross sectional areas of the branches. The areas are isolated by clustering and circles can be fitted. Circle center point, sphere center point and circle radius are used as cylinder parameters. The circle is enlarged after the cylinder parameter are stored and when transformed to a 3D sphere, the procedure can be repeated recursively until the complete tree structure is detected. The accuracy of the cylinder fitting is improved with Non-linear Least Squares (NLS) fit. Analysis of point to model distance showed that up to 99% of a tree can be modelled in average sub mm accuracy with this method.

The method was further improved in Hackenberg *et al.* [10]. Before the cylinder fitting routine is applied, input points are segmented into stem and branch points. By adjusting the method's input parameters according to the sub division a higher fit accuracy can be achieved. Combining the models' volume estimates with wood density values results in AGB predictions. Additionally various semi automatic de-noising procedures on imperfect point clouds were proposed. On 36 individuals of *Quercus petraea*, *Pinus massoniana* and *Erythrophleum fordii* comparison to ground truth AGB was performed. The total relative error (ERROR_REL) per species was 33.85%, 2.75%

and –17.24%. After applying a biomass expansion factor the total errors were reduced to 3.56%, 3.82% and –7.3% respectively.

Very few studies that model trees to a level of detail including thin branch-modelling exist, but have demonstrated the potential of utilizing tree skeletons as a basis for volume predictions. Point clusters belonging to the same cylindrical object can be generated by allocating points to their nearest skeleton segment. It is straightforward to generate cylinders from such clusters [12,13,49]. Therefore we include also works in this section focusing on the automatic extraction of the tree skeleton.

Bucksch *et al.* [51–53] stored TLS point clouds of trees in an octree structure. Neighbourhood information of octree cells were used to extract a graph. Cycles were removed from the graph, resulting in a representation of the skeleton of the tree. No relevant validation regarding forestry parameters was performed.

Bayer *et al.* [54] revealed the potential of QSMs to predict branch angles, branch length and branch bending. The authors utilized a manual skeletonization approach and also introduced the usage of alpha shapes [55] for accurate crown volume predictions.

Schilling *et al.* [56] described an automatic reconstruction technique utilizing 2D range images of trees. The 2D raster is subdivided into connected components. If the difference of range values between neighbouring points is smaller than some specified threshold, the points are considered to belong to the same component. With extended boundary tracing, the boundaries of the components are followed. A 2D skeleton is retrieved by applying a Voronoi Diagram, the components are further segmented according to their distance to the skeleton nodes. After the computation of principal curves, those are transformed to 3D to serve as polygonal lines of the final skeleton.

Delagrange *et al.* [57] proposed a method to extract tree skeletons utilizing Dijkstra's algorithm [41]. This approach of extracting objects skeletons from point clouds was firstly introduced by Verroust *et al.* [58]. Validation of this method was performed on summed up lengths of cylinder axes. Validation on an *Ulmus americana* L. of 2.5 m height revealed that the software could detect 85% of the branch axes. For four three year old saplings of the species *Acer saccharum* Marsh. and *Betula alleghaniensis* Britt. the error ranged between 2.2% and 9.1%.

1.1.2. Methods in Computer Vision producing QSMs of the Branching Structure

In the computer visualization—various efforts in this field have been done to model trees [59–62]—some of the basic principles of the presented methods have been developed. Instead of retrieving accurate forestry parameters, the objective of these works is a realistic appearance of the tree model in a computer rendered scene. A useful overview presenting also some of the history and background of these approaches is given in the thesis of Preuksakarn [63].

The usage of Dijkstra's algorithm for tree skeletonization occurred earlier in the field of computer vision than in computational forestry. For example Xu *et al.* and Livny *et al.* [64,65] used it for non validated tree skeletonization approaches. Neighbouring points are linked to each other resulting in a connected graph. On this graph Dijkstra's algorithm is applied to compute the minimal distance to a preselected root point for each point. Points belonging to the same distance bin are clustered and the centroids of neighbouring clusters are connected to build the tree skeleton.

The method we present here in the SimpleTree tool relies on Hackenberg *et al.* [10,12]. Here the idea of using sphere-surface cuts with point clouds of trees is utilized. This idea is based on Jayaratna [66] in the field of computer vision. To our knowledge the author invented the idea of a recursive search along the tree structure utilizing spheres. The base algorithm is quiet similar to the one presented here, which is also described in the appendix. A major difference in Jayaratna [66] to the SimpleTree approach is the circle fitting routine during the search for cylinders. The author fits planes into the cross-sectional areas of the branches. The intersection of those planes with the spheres serve as the detected circles, rather than fitting circles directly into the sub point cloud. A comparison of the effect of different circle fitting methods is performed in Hackenberg *et al.* [12]. Also none of the proposed post processing routines which improve the fit quality is performed in Jayaratna [66] as the visual results already satisfied the need of realistic looking models.

Another tree skeleton approach from this classical informatics field is the method of Yan *et al.* [67]. With the flooding algorithm [68] the point cloud is segmented into clusters. On each cluster a cylinder fitting routine is applied. In case no cylinder can be detected, another subdivision of the cluster into subclusters is performed, followed by a second cylinder fitting routine. The visual inspection revealed a gap-less cylindrical tree model.

Aiteanu *et al.* [69] fit ellipses into surface points utilizing the principal curvatures and principal directions of each points local neighbourhood. If a fitted ellipsis is not perpendicular to the branch axis an adjustment of the parameters is performed. Incorrectly detected ellipses are removed after being detected automatically. Between adjacent ellipses a cylinder surface is generated. The output model can be enriched with textured leaves.

1.1.3. Further Open Source Tree Modelling Software and Point Cloud Processing Libraries

Computree [70] is an open source platform utilizing TLS clouds. It is capable of generating a digital terrain model (DTM) on a plot level. Stems are detected by fitting circles with a Hough-transformation into slices of the vegetation points above the DTM. Circles in a spatial neighbourhood are combined to form stem models. Besides the DTM the output of Computree consists of a DBH estimator, a stem skeleton, a stem taper function and the height of each detected tree. Some of the algorithms implemented in Computree are described in detail in Othmani *et al.* and Ravaglia *et al.* [71,72]. The software framework allows developer-friendly implementation of methods due to its modular programming approach.

The work of Delagrange *et al.* [57] is available as an open source licensed Python script. A user interface allows access to adjust the earlier mentioned method with parameter modification. In addition, a visualization frame exists.

The increasing amount of publications in the LiDAR field is supported by a wide range of libraries. The Computational Geometry Algorithms Library [73] offers geometric algorithms for the computation of Voronoi diagrams, α-shapes, convex hulls and other structures. Both the Point Cloud Library (PCL) [74] and the Sorted Pulse Data software Library (SPDLib) [75] give access to methods specialized in the processing of LiDAR point clouds.

1.2. Relevance of the Presented Work in the State of the Art

Various authors [51–53,64,65,67] describe methods, where the potential to estimate AGB or wood volume was never validated. Delagrange *et al.* [57] only performed ground truth validation on young and small trees, while the height and size of a tree has a large influence on the modelling potential. The method of Côté *et al.* [42,44] was optimized for estimating the total leaf area and basal area instead of being trained on AGB predictions. The method of Belton *et al.* [47] was validated on only one individual without reliable ground truth, while the methods of Dassot *et al.* and Kankare *et al.* [13,14] rely on significant manual interaction. This is to be avoided to ensure the methods are as general as possible.

The software SimpleTree (installation instructions on the project homepage [76], source code on GitHub [77]) is an open source tool (BSD licence [78]) implementing the method presented in Hackenberg *et al.* [10,12]. Besides the method of Raumonen *et al.* [49], the SimpleTree method is the only QSM method validated for AGB estimates on a large number of trees without requiring a large amount of manual interaction. Other publications [13,14] contribute as well to the TLS based AGB prediction methods with a comparable sized data set. QSMs though have the beneficial potential to model also AGB distributions within a single tree individual, see Section 6. Those methods also do not rely on destructive harvested data to be trained [10].

The implemented method in SimpleTree was optimized regarding run-time efficiency and memory storage. New optimization methods, see Section 2.2, have been developed to improve the results presented in Hackenberg *et al.* [10]. The software is validated on data sets of 101 trees of six different species.

1.3. Structure of the Manuscript

Section 2 describes the functionalities of the presented software. SimpleTree results are compared to the results of the software tool relying on Raumonen *et al.* [49]. In Section 3 this comparison method is described. The utilized data sets are presented in Section 4. In Section 5 results of AGB estimations of both software tools are given. The results are discussed and interpreted in Section 6, leading to Section 8 where the relevance of the tool is debated. An outlook of possible future work is given in Section 7.

2. Software—SimpleTree

The method implemented in software SimpleTree is the one presented in Hackenberg *et al.* [10,12], a possible output is depicted in Figure 1. For all methods utilizing a TLS point cloud with n points the minimal expected runtime complexity of $\mathcal{O}(nlog(n))$ has been reached. The worst case complexity for the α hull computation is $\mathcal{O}(n^2)$ [55], but the input data is limited to the number of detected cylinders.

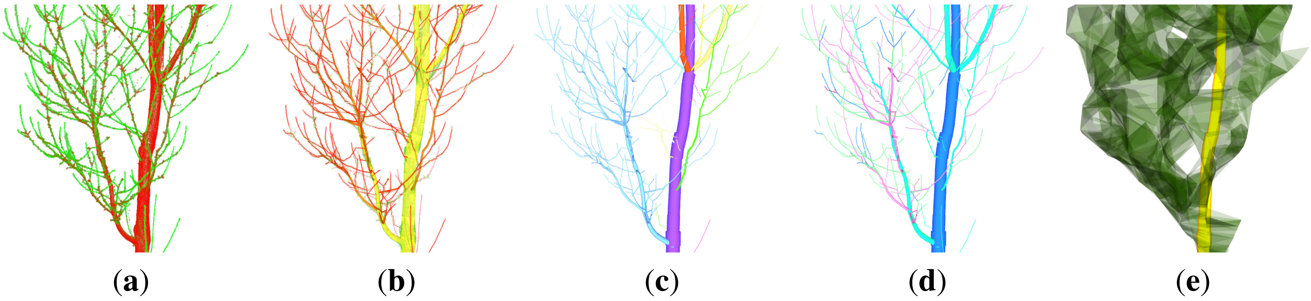

Figure 1. A QSM modelling with SimpleTree of a *P. avium* cloud: **(a)** the input cloud coloured by the second principal component [47]; **(b)** over 4500 cylindrical output features are coloured by the diameter of the represented AGB component; **(c)** secondary derived output features, *i.e.*, single branches, are coloured differently; **(d)** the branching order of the underlying tree component is coloured differently; **(e)** an abstract representation of the crown [54].

While the results of those publications were produced with a Java implementation, the presented version of software SimpleTree is written in C++. The PCL library [74] provides efficient functions for the implementation of the method. PCL's mathematical operations are based on the linear algebra library Eigen [79]. k-nearest neighbour searches are performed by the Fast Library for Approximate Nearest Neighbours (FLANN) [80]. PCL also ships with its own visualization library based on VTK (the Visualization Toolkit) [81].

For the user interface of software SimpleTree (Figure 2) the QT Framework [82] was utilized.

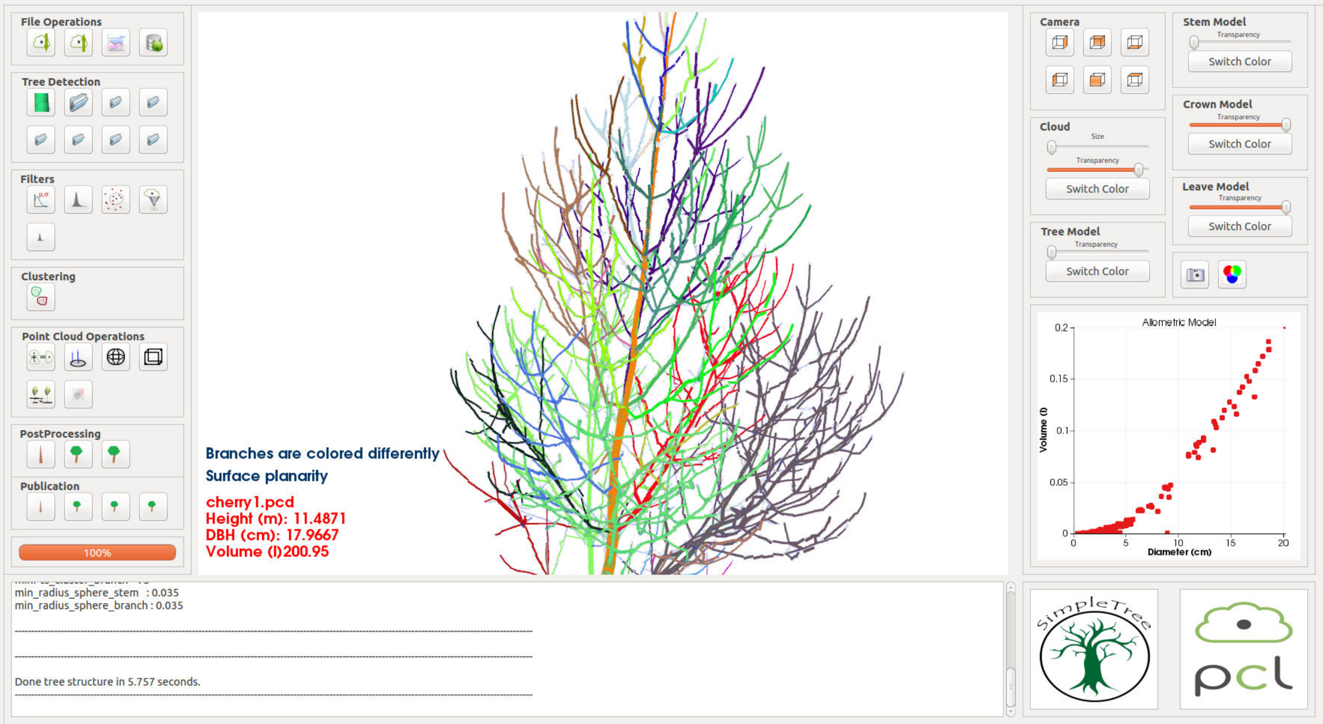

Branches are colored differently
Surface planarity

cherry1.pcd
Height (m): 11.4871
DBH (cm): 17.9667
Volume (l)200.95

```
min_radius_sphere_stem   : 0.035
min_radius_sphere_branch : 0.035

--------------------------------------------------------------------------------

--------------------------------------------------------------------------------

Done tree structure in 5.757 seconds.
--------------------------------------------------------------------------------
```

Figure 2. Screen-shot of the SimpleTree user interface.

The following sections describe methods provided by software SimpleTree. **Methodname** (*a, b*) is here-on a wild-card for a method with name **Methodname**, utilizing input parameters a and b. The dialogues utilized for user input of parameters include useful standard parameters, but to improve the results given by SimpleTree functionalities those standard parameters usually need to be adjusted to the point cloud quality.

2.1. Filter and Clustering Routines

Radius Outlier Removal (*r, k*) [83]

This method iterates over all points in the input cloud. For each point the number of neighbours inside a range *r* is computed. If a point has less than *k* neighbours, it is removed from the point cloud.

Statistical Outlier Removal (*sdMult, k*) [83]

This method iterates over all points in the input cloud. For each point the average distance to its k nearest neighbours is computed. Mean m and standard deviation sd are calculated for those distances. If a point's average distance is larger than $m + sdMult \times sd$ or smaller than $m - sdMult \times sd$, it is marked as an outlier and removed from the cloud.

Voxel Grid Filtering (*cellsize*) [83]

This method is an information loss reduced down-sampling approach. Over the point cloud a three-dimensional voxel grid is generated. The cell size of the voxels equals $cellsize$. If a voxel contains at least one point, for the output cloud a point is generated. The output point is the centroid of all contained points, which minimizes the information loss of the down-sampling procedure compared to using the voxel center point.

Curvature Filtering (*min1, max1, min2, max2, min3, max3*)

A PCA is performed for each point's neighbourhood. λ_1, λ_2 and λ_3 denote the normalized Eigenvalues for each point. For all λ_1 minimum min and maximum max value are computed. $min1$ and $max1$ are percentage numbers. A point is considered an outlier, if its λ_1 is smaller than $min + (max - min)/100 \times min1$ or larger than $min + (max - min)/100 \times max1$. λ_2 and λ_3 are processed in the same manner. The thresholds are adjusted with a slider and before the removal-confirmation all noise points are marked via transparency and colourisation in real time according to the slider values (Figure 3).

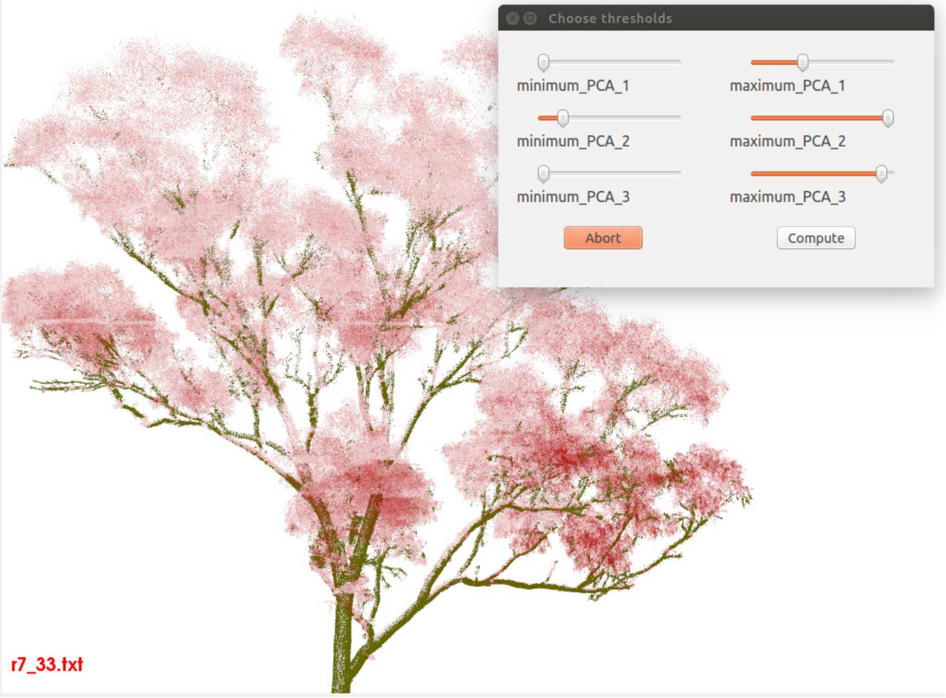

Figure 3. Usage of curvature filtering routine. Outlier points, *i.e.*, non woody material points, are coloured red transparent.

Intensity Filtering (*min, max*)

All points whose intensity is smaller than min or larger than max are marked as outliers and are removed from the cloud. The thresholds are adjusted with a slider and before confirmation the points which will be deleted are visualized with a red, transparent color.

Crop Sphere | Crop Box (*radius*)

A manual noise removal tool which generates a sphere. The center point can be set on any cloud point by mouse interaction. The sphere $radius$ can be adjusted too. After confirmation, all points inside the sphere are removed from the cloud. A similar tool utilizing a box instead of the sphere exists in addition.

Euclidean Clustering (*clusterTolerance, minPts, numCluster*) [83]

A simple but fast spatial clustering operation is applied. The output cloud will contain the $numCluster$ largest clusters containing at least $minPts$ points. If only a smaller number of clusters exists, $numCluster$ is set automatically to this number. Points are separated into two clusters, if the distance between the closest point pair exceeds $clusterTolerance$. This operation is faster than the Density-Based Spatial Clustering of Applications with Noise (DBSCAN) [84], which was used in Hackenberg *et al.* [10,12].

2.2. Tree Modeling

Stem Point Detection [10] ()

The stem point detection does not use input parameters. A PCA is performed on each input points neighbourhood of a **Voxel-Grid** (0.02) filtered input cloud. If the eigenvalues λ_1, λ_2 and λ_3 fulfil user-hidden thresholds, the point is accepted as a preliminary detected stem point. On these points **Euclidean Clustering** (0.05, 1, 100) is performed and the output is marked as further detected stem-points. By a simple buffering operation (buffer width = 0.05 m) with the original cloud, the original cloud can be enriched with stem point information. Downscaling and up-scaling was not used in [10] and is now included to improve runtime performance.

Spherefollowing Method [10,12] (*sphereMultiplier, epsClusterStem, epsClusterBranch, epsSphere, minPtsRansacStem, minPtsRansacBranch, minPtsClusterStem, minPtsClusterBranch, minRadiusSphereStem, minRadiusSphereBranch*)

The method is used to fit cylinders into a de-noised point cloud and to build the tree model. Stem points should be detected before running this method. Spheres are utilized to follow the branching structure of the tree from the root to its tips.

A sphere with a center point on a skeleton axis cuts the point cloud. All points within a distance of $epsSphere$ to the sphere-surface are considered to be used to detect the next sphere and are put into a sub point cloud P_{sub}. P_{sub} is subdivided into P_{Stem} and P_{Branch}. P_{Stem} (P_{Branch} is processed in same manner) is clustered then with **Euclidean Clustering** ($epsClusterStem$, 5 ,$minPtsClusterStem$) into i clusters P_i. The number of returned clusters is set to five, as this is the maximum expected number of cross sectional areas located on a sphere surface. Each cluster represents a cross-sectional area of the stem/branch. A circle is fitted with the Random Sample Consensus (RANSAC) [85,86] algorithm into P_i, if the number of points in P_i exceeds $minPtsRansacStem$, and with the more robust but less accurate median method proposed in Hackenberg *et al.* [12] otherwise. The center point of the circle, the center point of the sphere and the circle radius are chosen as cylinder parameters. The circle is enlarged with $sphereMultiplier$ and transformed to a three dimensional sphere. The procedure is repeated recursively until no more cross sectional areas can be found.

The detected cylinders are improved with RANSAC [85] algorithm, the former Java implementation utilized NLS fit. More details on the method itself and further post-processing steps on the detected cylinders are given in Hackenberg *et al.* [10,12], as well as in the Appendix D.

Parameters extractable from the final tree model are discussed in the section output.

Parameter Optimization (*iterations, criterion, seeds*)

The **Spherefollowing Method** uses ten input parameters. To enable an automatic search for optimal parameters, initial parameters have to be set by the user. Then a multi-threaded parameter search starts. In each iteration step $seeds$ new parameter sets are created. For one creation each parameter is chosen from a normal distribution centred around the parameter value from the last iteration. For each set a tree model is build. The average euclidean distance from the point cloud to the model is computed. If this distance is smaller than the last found optimal distance, the method stores the distance and the parameter set. If after one iteration the distance improvement is smaller than $criterion$, the search is stopped. If the number of iterations exceeds $iteration$, the search stops. The best parameter set is printed out after completion.

Allometric improvement (*a, b, fac, minRad*)

A new parameter named $GrowthVolume$ is generated for each cylinder. The $GrowthVolume$ of a cylinder is the cylinder's volume plus the $GrowthVolume$ of all the cylinder's children. If analysed against the radius of the cylinder, an allometric model of the form $y = ax^b$ can be fitted via NLS fit.

Figure 4(a) depicts this analysis for a *Prunus avium* model. The point cloud is of high quality and so are the models [12]. The coefficient of determination (R^2) for this model is 0.979, revealing a strong natural pattern un-discussed in computational forestry. It needs to be mentioned, that the usage of the R^2 for non linear model fits is criticized [87]. Still many commercial software packages, *i.e.*, Prism, Origin, Matlab, SPSS and SAS, calculate the R^2 for non linear fits.

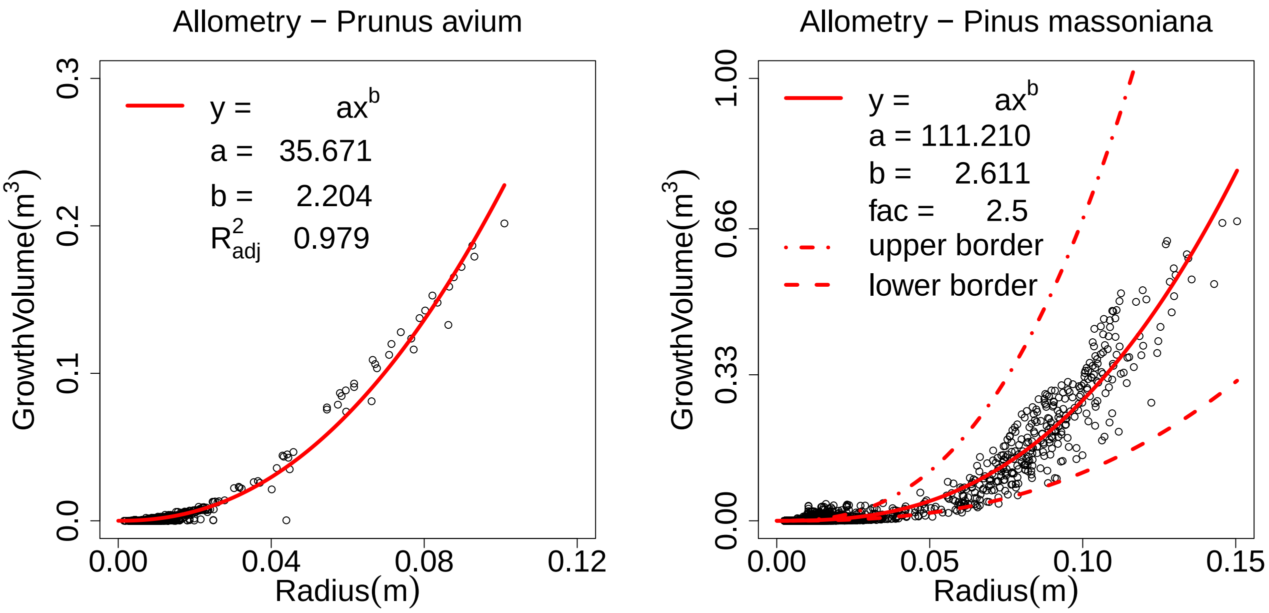

(**a**) (**b**)

Figure 4. An allometric model derived from: **(a)** a single *Prunus avium*; **(b)** twelve *Pinus massoniana*.

The parameters a and b need to be computed externally (an R-script is provided on the project home page). The method can detect overestimated cylinders as outliers of this function, see Figure 4(b) for poorer quality models which need the allometric improvement. Outliers are considered the cylinders with a *GrowthVolume* smaller than their predicted *GrowthVolume* divided by fac. Their radii are adjusted to be in accordance with their fixed *GrowthVolume*.

All cylinder radii smaller than *minRad* are set to *minRad* in a last step. If this method is combined with the **Parameter Optimization**, the minimum radius can be automatically computed.

Crown Computation (α)

Modelling the crown as a convex hull utilizing cylinders as input data was already proposed in Hackenberg *et al.* [12,88], Figure 5(a).

In addition, α-shapes [55] can be generated, as suggested in Bayer *et al.* [54]. For the α-shape generation of a point cloud an input parameter α is needed. If α is zero, the shape is the point cloud itself, for an α value near ∞ the shape is the convex hull. Figures 5(b) and 5(c) depict different α-shapes with values 0.2 and 0.1.

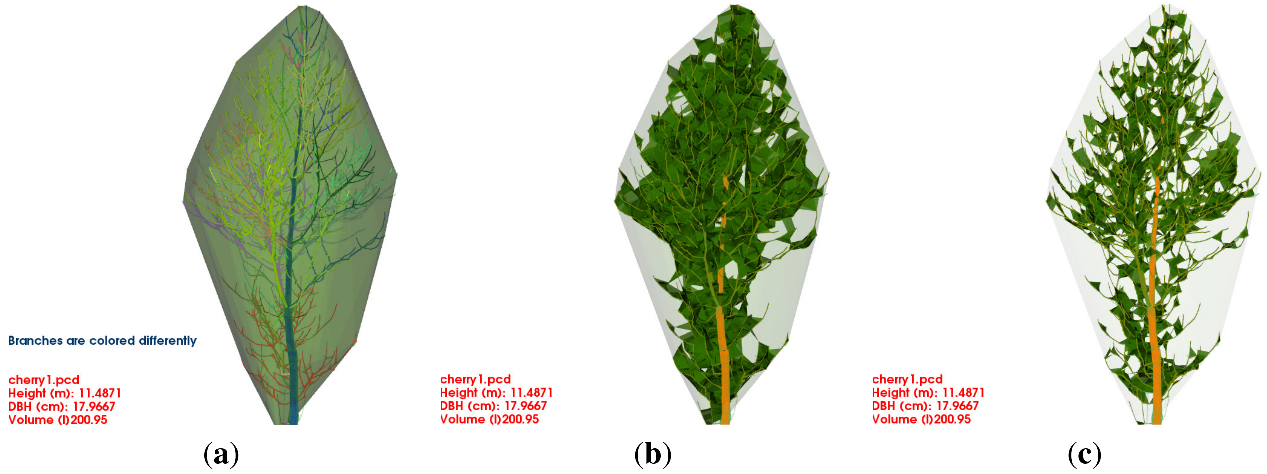

(**a**) (**b**) (**c**)

Figure 5. Different crown models for a *Prunus avium*: **(a)** the convex hull; **(b)** the α hull with $\alpha = 0.2$; **(b)** the α hull with $\alpha = 0.1$.

With an appropriate α-value the modelling of the leaf-space occupation is possible [54].

2.3. Point Cloud Processing

Iterative Closest Point (ICP) (β) [74,89]

ICP is an algorithm for aligning two different point clouds representing the same object proposed in Besl and McKay [89]. The algorithm is supposed to be executed successfully, if the clouds are initially aligned, Figure 6(a)–6(d).

The initial alignment is performed in two steps. Both clouds are automatically transformed, so that the base of each tree is in the origin of the coordinate system, Figure 6(a). Afterwards the source cloud is rotated with angle β around the z-axis. The angle can be manually found out by using a slider for its value with in-real-time visualized rotation update, Figure 6(b). Then the ICP algorithm can be started, Figure 6(c), 6(d). Aligning two clouds of the same tree from different time-stamps with ICP was also proposed in Kaasalainen *et al.* [8].

Merge ()

This function merges two point clouds.

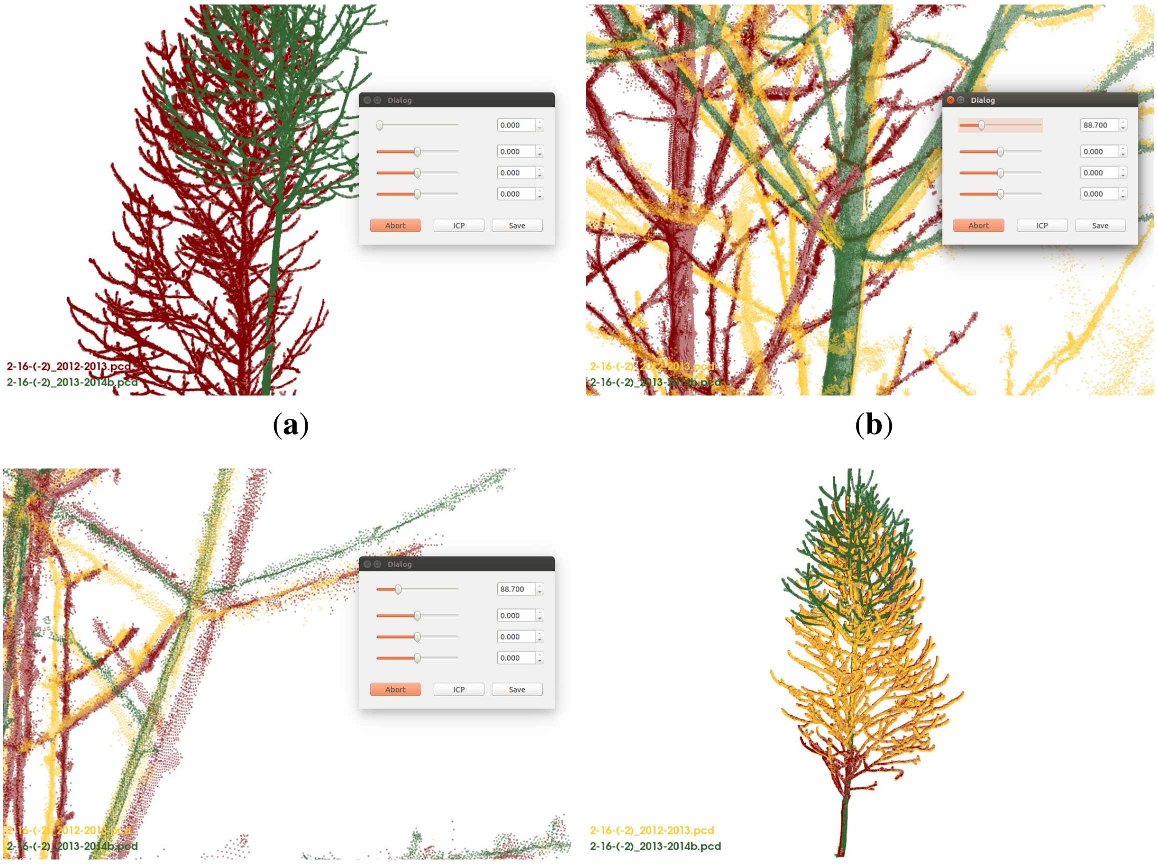

(**a**) (**b**)

(**c**) (**d**)

Figure 6. Alignment of a *P. avium* cloud [12] of winter 2012 to the cloud of of the same tree after pruning in winter 2013: **(a)** red cloud (2012) and green cloud (2013) are automatically initial aligned; **(b)** red and green cloud are the same as in **(a)**, the yellow cloud (2012) is a manually rotated version of the red cloud; **(c)** the final result - the green cloud is the target cloud and the red one the manually aligned cloud and the yellow cloud the ICP improved version of the red cloud; **(d)** the final result from another point of view.

2.4. Output Data

Multiple output files are generated.

Cloud To Model Distance

This file contains one entry per point in the input cloud. The entry is the minimum distance from the point to the model. For performance reasons the maximum distance is 0.1 m, if the real distance is larger than this value, the entry will be 0.1 m.

Single Value Tree Parameters

This file contains the entries for the total tree volume and the stem volume. Solid volume is the volume of all compartments with a diameter larger 7 cm. The tree's height and its length are included, as well as the DBH and the root diameter at lowest z-coordinate. The stem volume from the root up to the first branch and the stem volume up to the crown base are printed with additionally the crown base height. The crown volume and the crown surface from the convex hull crown model and lastly the crown projection area are additional output parameters. In Hackenberg *et al.* [12] more detailed definitions on various output parameters are given.

Complete Cylinder Model

This file contains one entry per row for each cylinder consisting of: x,y,z-coordinates of start and end point, as well as the radius. Length and volume, also computable from the first named parameters, are included, a unique segment ID of the segment containing the cylinder next, as well as this segment's parent segment ID. The segment ID with the parent information allows the full reconstruction of the tree structure in external software, as cylinders are stored in the order in which they occur in the segment. Therefore the stored branch ID is also already computable meta-data. The growth volume is saved, as well as the branch order.

3. Software—Comparison Method Raumonen *et al.* (2013)

The results of SimpleTree applied to destructively sampled estimates will be compared against the results of the approach of Raumonen *et al.* [49]. There are two main procedures in this method [49]: first the point cloud is segmented into stem and individual branches, and then the segments are approximated with cylinders or other fundamental geometric primitives. For the segmentation, the point cloud is partitioned into small subsets, which correspond to small connected patches in the tree surface. The partition into patches and the segmentation are done twice: first large uniform size patches give a rough approximation of the local branch sizes and the branching structure. The actual patch sizes used in this first segmentation are relatively insensitive and in this paper we used patches whose minimum diameters was set to 12 cm (the size randomly varies between the given minimum and twice the minimum). This first segmentation then determines the variable sizes of the patches in the second partition, which is used for a more detailed segmentation. The user given minimum diameters at the base of the stem and tips of the branches determine the sizes of the patches in the second partition. In this paper we set the minimum diameters at the base to 8 cm and at the tips to 1 cm.

Each segment is approximated with cylinders that are fitted in the least squares sense to small sub-segments. The ratio between length and radius of the sub-segments is roughly equal to a user given input. Also the initial radii of the sub-segments are estimated and based on the estimated radii outlier points are removed. After the fitting of the cylinders into a segment, the radii are checked to correct too large and too small radii: partially linearly decreasing tapers for the stem and parabolic tapers for the branches are used to give the local maximum and minimum radius. The tapers are estimated from the fitted data for the first $3/4$ of the branch length and at the tip of the branch the radius is set to small maximum value [9].

Additionally, the SimpleTree **Allometric improvement** was used in a second statistical improvement instead of the taper improvement. Parameters a and b were directly computed per model within the Matlab code with the standard Matlab NLS fitting routine.

The partitions into patches are random and thus each modelling run results in small differences in segmentation and thus in small differences in the resulting QSM. To estimate the variability of the result we made 500 models from one of the trees with the same input parameters and the distribution of total volumes of these models is shown in Figure 7.

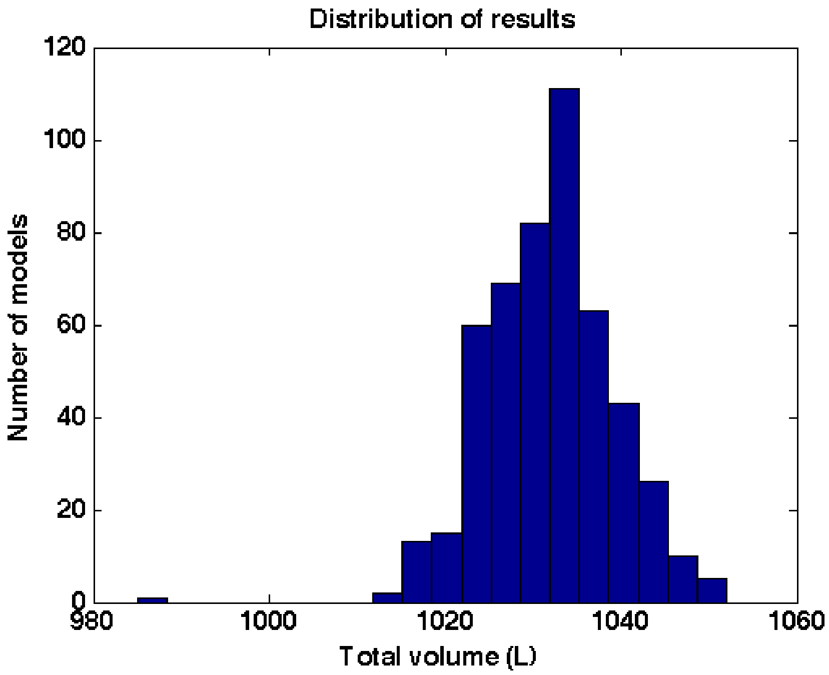

Figure 7. Distribution of total volumes of 500 QSM models made with the same input parameters.

This distribution is taken then as an approximation of the real model result distribution and to estimate the sample size effects we can use it for simulated sampling: For each sample size, from 1 to 30, we took 10000 random samples and computed the sample means. Figure 8 shows the variations of the sample means for each sample size and with sample size five or higher the maximum difference to the actual mean is about 1.5% and the standard deviation is about 0.3% of the mean. Thus five models are enough to reach small variability in the sampling. In this paper five models were computed and the results shown are the averages with standard deviations computed from the five models.

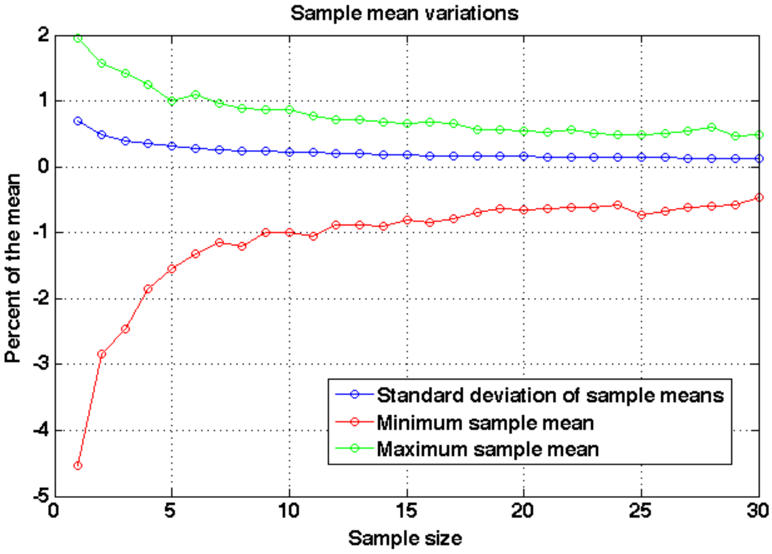

Figure 8. The variation of the sample means as a function of sample size. The standard deviation and the difference of minimum and maximum sample means are given as percentages to the mean of the distribution.

All the models were based on fixed patch diameters described above and only the relative cylinder length and the relative radius for outlier point removal were selected with the following simple optimization procedure: we made the models for all the parameter combinations and then selected the optimum based on the median point-to-model distances. The values for the relative cylinder lengths were 2, 3, 4 and 5. The values for the relative radius for the outlier removal were 1.5, 2.0, 2.5, 3.0 and 3.5 (*i.e.*, all the points whose distance from the estimated cylinder axis is over 3.5 times the estimated radius are removed).

4. Data Sets

Four data sets of different tree species, *i.e.*, *Erythrophleum fordii*, *Pinus massoniana*, *Quercus petraea*, *Eucalyptus leucoxylon*, *Eucalyptus microcarpa* and *Eucalyptus tricarpa*, with destructively harvested AGB have been used to validate software SimpleTree. *Erythrophleum fordii*, *Pinus massoniana* and *Quercus petraea* clouds were presented firstly in Hackenberg *et al.* [10] and can be obtained under Creative Commons Non Commercial Share Alike 4.0 [90] from the data section in the project homepage [76]. The point cloud post processing with SimpleTree is described in the Appendix A. The volumes of reconstructed trees were multiplied with density values discussed in Wassenberg *et al.* [91] to estimate biomass.

4.1. E. fordii

Twelve *Erythophleum fordii* were scanned with the Z+F IMAGER 5010c [92] in October 2013 in sub tropical China. Due to the evergreen nature of those trees the clouds contain a large amount of points on the leaves of the trees. The trees were 32 years old when harvested and came from a pure stand. The selection of twelve individuals was performed in a manner that on one hand a wide range of the DBHs was achieved and on the other hand the damage done by destructive harvesting was considered to be minimized.

4.2. P. massoniana

Twelve *Pinus massoniana* were scanned with Z+F IMAGER 5010 [93] in March 2013 in sub tropical China. The scans were affected by wind. In addition, the needles of the coniferous trees added noise to the scans. The pure stand was planted 21 years before the harvesting took place. Similar to the selection process of *Erythophleum fordii* both DBH variety and minimization of damage were taken to account.

4.3. Q. petraea

Twelve *Quercus petraea* were scanned with the Z+F IMAGER 5010 [93] in February 2014 in southern Germany. All trees were scanned in leaf condition off. The scans were affected by wind and rain. At the time of the harvesting the trees were 93 years old. Due to the destructive harvesting no high quality timber trees have been selected from the pure stand.

4.4. Eucalyptus Leucoxylon, Eucalyptus Microcarpa and Eucalyptus Tricarpa

TLS data of three Eucalyptus species were collected in May 2012 in Rushworth forest, Victoria, Australia. In this native open Forest two plots were selected, with a basal area of 13.0 m^2/ha and 13.2 m^2/ha respectively. The data were acquired with a RIEGL VZ-400 terrestrial laser scanner (RIEGL Laser Measurement Systems GmbH). 65 trees were destructively sampled and reference estimates of AGB were collected. Individual trees were extracted from the TLS data and used to validate the QSM approach of Raumonen *et al.* [49] in Calders *et al.* [9]. The reader is referred to the latter publication for full details of the TLS and destructive harvesting data collection and processing.

5. Results

The effect of the parameter optimization was analysed. All manual de-noised clouds of *Q. petraea* were modelled five times with **Parameter Optimization** (*iteration*, 0.0001, 81). In six different runs *iteration* was set to 0, 1, 2, 4, 6 and 8. The **Spherefollowing Method** (1.8, 0.035, 0.015, 0.025, 500, 1111200, 12, 3, 0.07, 0.03) was additionally improved with the **Allometric improvement** (240.559, 2.72, 2.5, 0.0025) in the optimization routine. The average standard deviation of the AGB volume prediction per tree in m^3 of five model runs with a fixed number of iteration was calculated first (Figure 9(a)).

The total relative error (Error) of the mean value of the five predictions was computed (Figure 9(b)), as well as the average coefficient of determination ($R^2_{adj.}$) of the five linear models with the form

$$y = ax + b \tag{2}$$

with x being the TLS derived biomass and y being the ground truth biomass, see Figure 9(c). In Figure 9(d) the influence of $iterations$ on the CCC between ground truth and TLS predicted biomass is depicted.

Visualization in addition revealed, that with increasing *iterations* parameter, more crown branches can be detected (Figure 10). No negative side effects were observed, *i.e.*, no non existing branches were added to the models.

By detecting the majority of the last remaining undetected branches during the modelling, the total relative error of the biomass prediction rises. Without the **Parameter Optimization** (...) the overestimation for twelve *Q. petraea* trees is $\sim 1\%$, the error stabilizes at a maximum of $\sim 5\%$ with at least four iterations of the **Parameter Optimization** (...).

With only one iteration in the **Parameter Optimization** (...), the ERROR_REL is $\sim 3\%$, leaving an estimated $\sim 2\%$ of total biomass undetected. The accuracy of the AGB volume prediction is with one iteration yet unstable, as the average value for the standard deviation of one tree modelling is $\sim 0.03m^3$, while it can be reduced to $\sim 0.01m^3$ with at least one more iteration.

The adjusted coefficient of correlation ($R^2_{adj.}$) is with any number larger one of iterations improved to a value of ~ 0.85 instead of ~ 0.75.

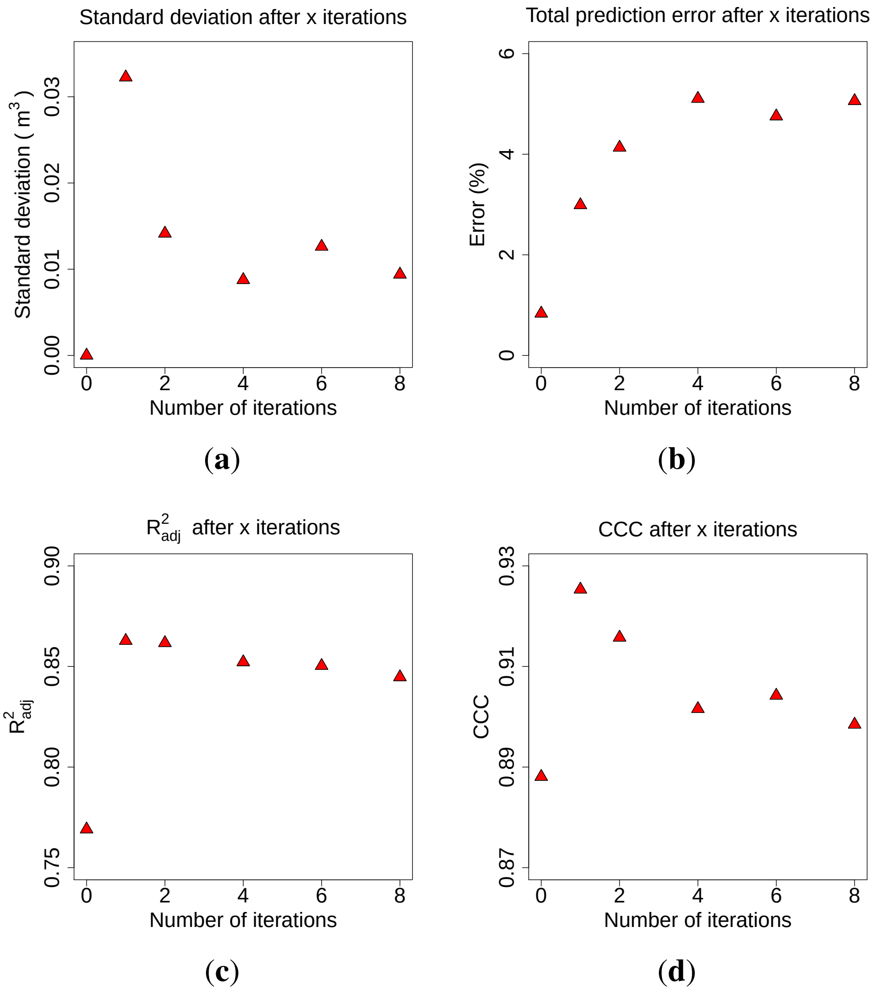

Figure 9. Impact on the number of iterations during parameter search on: **(a)** the average standard deviation of the volume prediction on tree level; **(b)** the average total relative error of the biomass prediction on complete data set level; **(c)** the $R^2_{adj.}$ of the model predicting ground truth biomass from TLS derived biomass; **(d)** the CCC between ground truth and TLS predicted biomass.

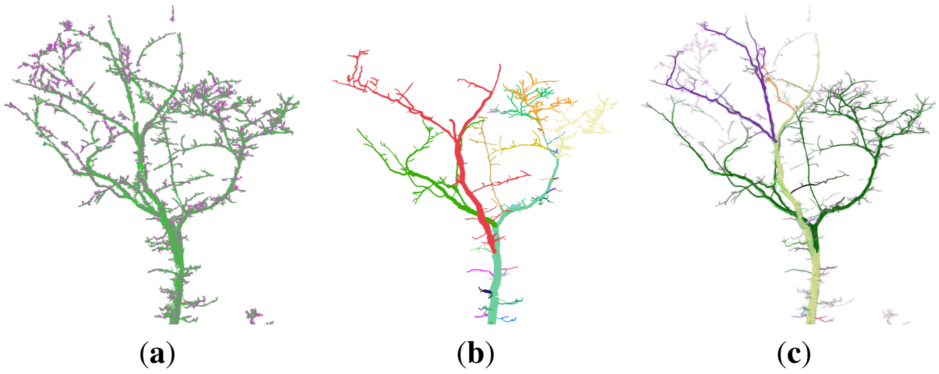

Figure 10. Visualization of the modelling of a *Q. petraea* **(a)** the input cloud; **(b)** the model with unoptimized parameters; **(c)** the model with optimized parameters (six iterations).

With **Parameter Optimization** (≥4, 0.0001, 81) the majority of AGB is successfully detected. There seems to be a systematic error of $\sim 5\%$ overestimation in the modelling of the *Q. petraea*. The prediction accuracy on tree level is quantified by a $R^2_{adj.}$ value of ~ 0.85. The systematical error results in a reduction of the CCC to ~ 0.9 though, as the overestimation of five percent is hidden by the fact that not all branches are detected with only one iteration, where the CCC reaches its maximum of ~ 0.93.

The computation for the analysis, consisting of more than 100,000 tree modelling runs computed within less than three days on seven Intel(R) Core(TM) i7-2600K CPU @ 3.40GHz cores (Intel, Santa Clara, CA, USA).

In addition, the effect of the **Allometric Improvement** (240.559, 2.72, 2.5, 0.0025) was analyzed (see Figure 11). The twelve *Q. petraea* were modelled one time with the statistical improvement and one time without. Each modelling run of the complete data set took ~10 min. The parameters a and b were computed from the non improved data set, fac was estimated by visual inspection of the same plot (Figure 11(a)). The $minRadius$ was set in a manner, that the tip of the branches had a minimum diameter of half a centimetre (Figure11(c)), 11(d)).

The outlier cylinders, whose $GrowthVolume$ is larger than the threshold depicted by the upper border in Figure 11(a), were not modified. Still such outliers don't occur in Figure 11(b) and we conclude, that only erroneous cylinders with overestimated radii exist and have to be handled. The outliers outside the upper border are derived from the inclusion of multiple child relation cylinders with overestimated radii in the computation of their respective $GrowthVolume$. Additionally it is stated, that the curvature of the allometric function is enlarged by the appliance of this statistical improvement.

A linear model of the form of Equation (2) is calculated for both data sets. The $R^2_{adj.}$ for the unimproved data is 0.59, applying the **Allometric Improvement** (...) leads to a value of 0.85. The overestimation of ~25.89% is reduced to ~2.42% with the improvement. The CCC rises from 0.45 to 0.92 (Figure 11(e), 11(f)).

In the same manner results are computed for the *P. massoniana*. The scans were modelled with the **Spherefollowing Method** (3, 0.035, 0.025, 0.02, 200, 1111200, 3, 5, 0.07, 0.05). In one run with **Allometric Improvement** (137.498, 2.62, 2.5, 0.0025) inside the **Parameter Optimization** (6, 0.0001, 81) search (Figure 12(b), 12(d), 12(f)) and one time without those improvements (Figure 12(a), 12(c), 12(e)). In the comparison to the ground truth data the $R^2_{adj.}$ was improved from 0.81 to 0.95, the ERROR_REL reduced from 34.63% to 3.59% and the CCC improved from 0.65 to 0.97. The calculation with the **Parameter Optimization** (...) took ~3.5 h, the other ~10 min.

The *E. fordii* scans were modeled with the **Spherefollowing Method** (1.5, 0.03, 0.02, 0.02, 10, 10, 3, 3, 0.07, 0.025). In one computation the **Allometric Improvement** (95.551, 2.5, 2, 0.015–0.025) inside the **Parameter Optimization** (6, 0.0001, 81) search was performed, a second run excluded those improvements.

Twig points have been near completely removed due to coverage by leaves, as show in Hackenberg *et al.* [10]. Therefore the minimum radius in **Allometric Improvement** (...) was set to a value derived from the automatic parameter search to prevent the smaller branches treated as twigs (Figure 13(a)). Additionally, an NLS model of the form

$$y = ax^b + c \tag{3}$$

was fitted on the improved data (Figure 13(b)). c was utilized as an additive component on biomass estimators to account to the removal of twigs. In the comparison to the ground truth data the $R^2_{adj.}$ was improved from 0.80 to 0.92, the ERROR_REL reduced from –14.92% to –4.59% and the CCC improved from 0.80 to 0.92 (Figure 13(a), 13(b), 13(e), 13(f)). The calculation with the **Parameter Optimization** (...) took ∼2 h, the other ∼10 min.

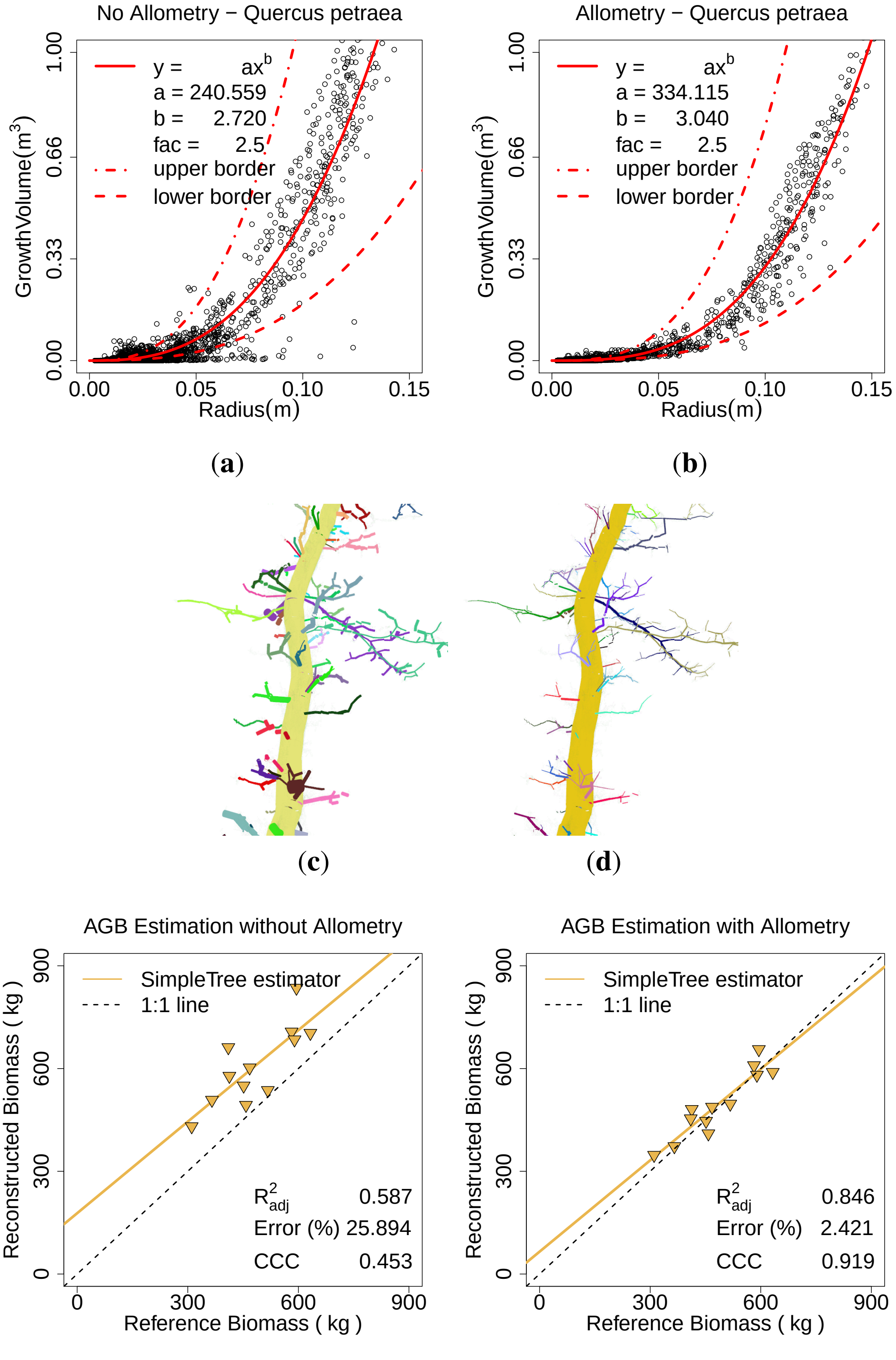

(**a**) (**b**)

(**c**) (**d**)

(**e**) (**f**)

Figure 11. Effect of the allometric improvement on *Q. petraea*: **(a)** the fitted model based on the unimproved data; **(b)** the fitted model based on the improved data; **(c)** the model visualization without the improvement; **(d)** the model visualization with the improvement; **(e)** AGB estimation without the improvement; **(f)** AGB estimation with the improvement.

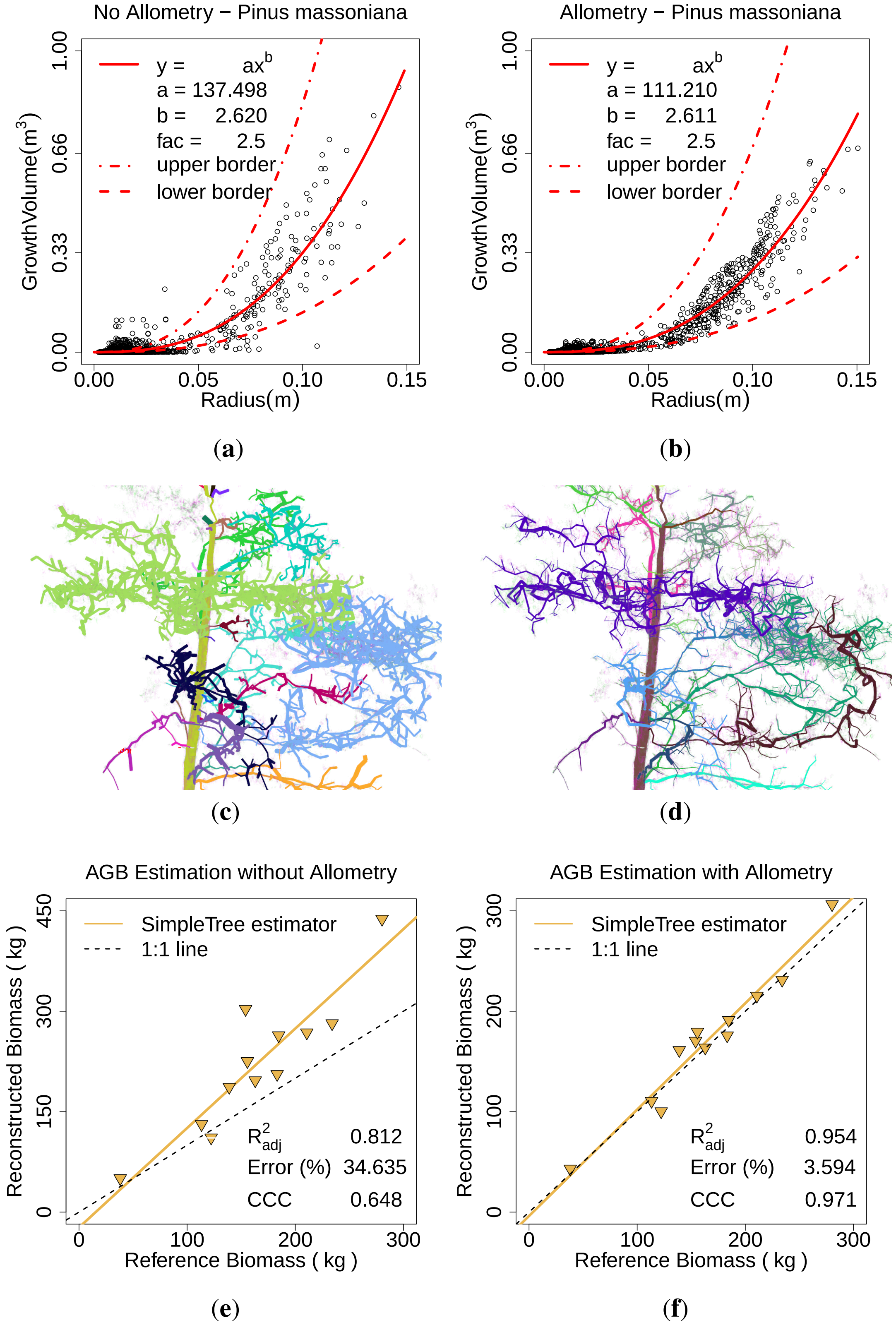

(**a**) (**b**)

(**c**) (**d**)

(**e**) (**f**)

Figure 12. Effect of the allometric improvement and the automatic parameter search on *P. massoniana*: **(a)** the fitted model based on the unimproved data; **(b)** the fitted model based on the improved data; **(c)** the model visualization without the improvement; **(d)** the model visualization with the improvement; **(e)** AGB estimation without the improvement; **(f)** AGB estimation with the improvement.

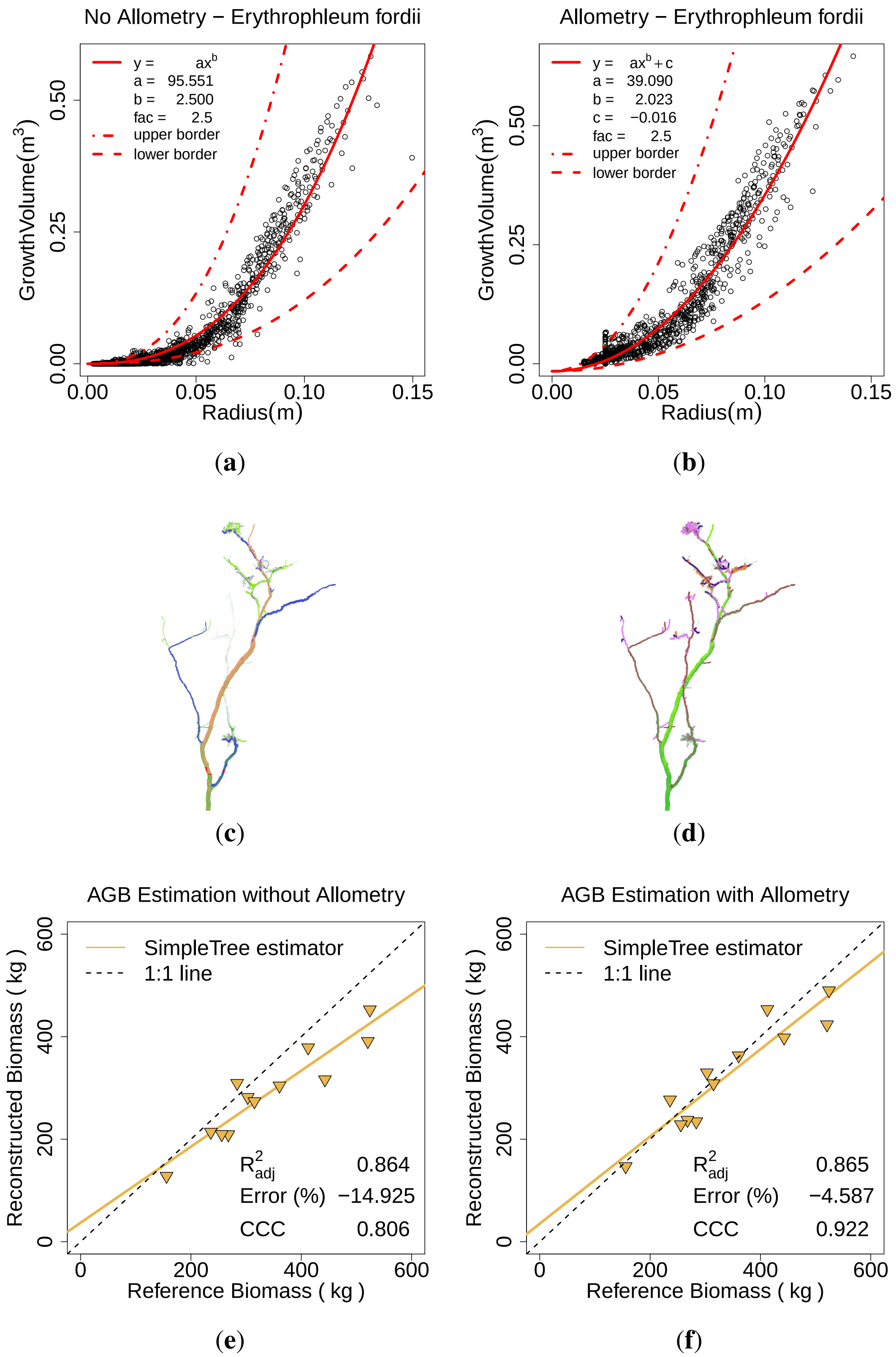

Figure 13. Effect of the allometric improvement and the automatic parameter search on *E. fordii*: **(a)** the fitted model based on the unimproved data; **(b)** the fitted model based on the improved data; **(c)** the model visualization without the improvement; **(d)** the model visualization with the improvement; **(e)** AGB estimation without the improvement; **(f)** AGB estimation with the improvement.

All three data sets (*E. fordii*, *Q. petraea* and *P. massoniana*) have additionally been modeled with the comparison QSM approach of Raumonen *et al.* [49] in three different manners. One time the cylinder radii have not been adjusted statistically, one time the taper correction has been used and one time the allometric improvement was utilized (Figure 14).

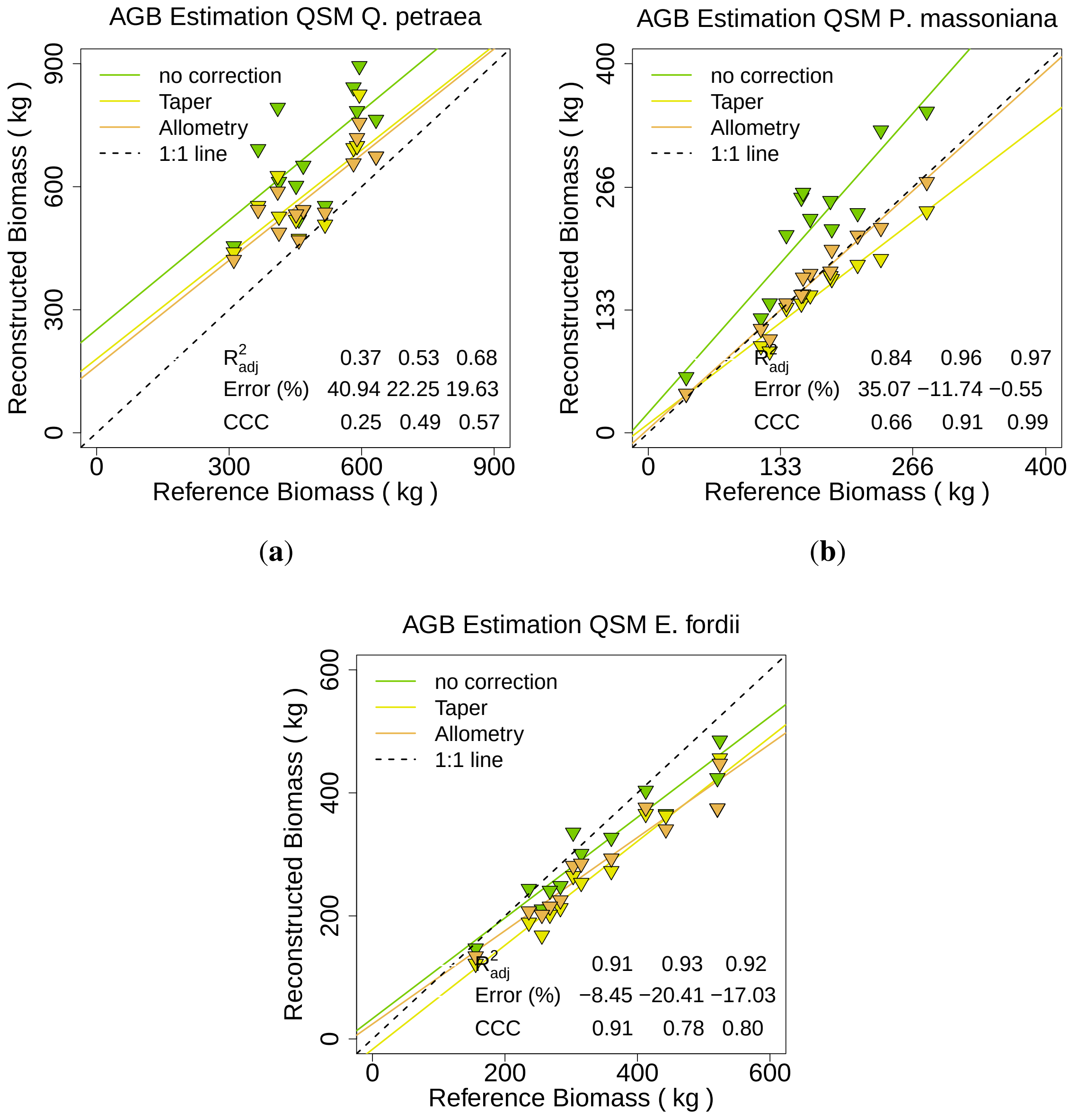

(**a**) (**b**)

(**c**)

Figure 14. Effect on different statistical radii adjustments in the Raumonen *et al.* approach [49] for: **(a)** *Q. petraea*; **(b)** *P. massoniana*; **(c)** *E. fordii*.

For *Q. petraea* and *P. massoniana* the approach without radius correction revealed a large overestimation for both species (41% and 35%). The $R^2_{adj.}$ (0.37 and 0.84) and CCC (0.25 and 0.66) both had the lowest values with this modelling approach. The taper correction reduced the overestimation (ERROR_REL of 22% and –12%) as well as it improved the $R^2_{adj.}$ (0.53 and 0.96) and the CCC (0.49 and 0.91). Best results were produced by applying the allometric improvement, reducing the ERROR_REL further (20% and –1%), improving the $R^2_{adj.}$ (0.68 and 0.97) as well as the CCC (0.57 and 0.99). For

E. fordii the ERROR_REL was lowest in the no improvement result (-9% instead of –21% for the taper correction or –17% for the allometric approach). The $R^2_{adj.}$ was approximately stable over all three runs (0.91, 0.93 and 0.92), the CCC due to its Error influence best for the no correction approach (0.91 instead of 0.78 or 0.80).

For all four data sets SimpleTree results are compared directly against the Raumonen *et al.* [49] results. For both methods the manual de-noised data sets of *P. massoniana*, *Q. petraea* and *E. fordii* have been utilized. The Raumonen *et al.* [49] results have been improved in all three cases with the allometric approach, although for *E. fordii* better CCC could have been achieved without corrections. The *Eucalyptus spp.* data set was handled differently. The Raumonen method results have been taken from Calders *et al.* [9]. For the SimpleTree results manual de-noised data has been used with a **Parameter Optimization** (*6, 0.0001, 81*) utilizing the same parameter set for all 65 trees in the **Spherefollowing Method** (*3.0, 0.1, 0.1, 0.045, 200, 1200, 3, 3, 0.1, 0.1*). Parameters a and b were considered poor in the allometric improvement, as the NLS model did not show high quality as other allometric models did (Figure 15).

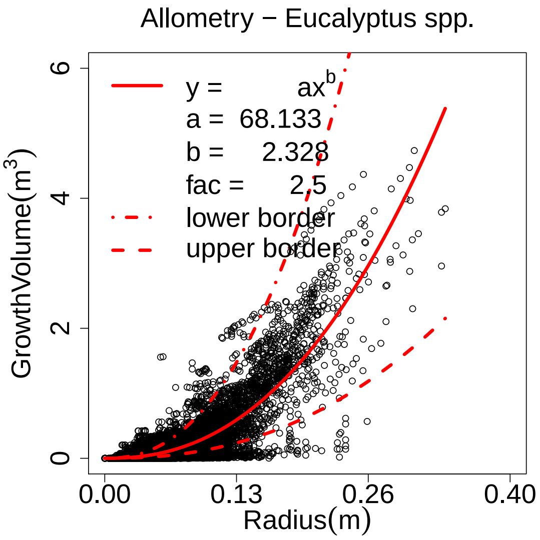

Figure 15. Allometric function for all utilized Eucalypt species.

For *P. massoniana* the Raumonen *et al.* [49] results revealed an CCC of 0.99, SimpleTree results a CCC of 0.97. *Q. petraea* results revealed with the Raumonen *et al.* [49] approach 20% overestimation, resulting in a CCC of 0.57. SimpleTree results could achieve a CCC of 0.92 at the modelling of this species. *E. fordii* scans with removed twigs resulted in an underestimation for both species. The CCC is 0.80 for the Raumonen *et al.* [49] results and 0.92 for SimpleTree. For *Eucalyptus spp.* the CCC of Raumonen *et al.* [49] modelling is 0.98 and 0.94 for the SimpleTree results (Figure 16). In addition, a final comparative result was produced including all 101 trees of the six species (Table 1).

Table 1. Results for all six analysed species.

Method	Error	$R^2_{\text{adj.}}$	CCC
Raumonen *et al.* (**2013**) [49]	8.80	0.97	0.98
SimpleTree	7.24	0.91	0.95

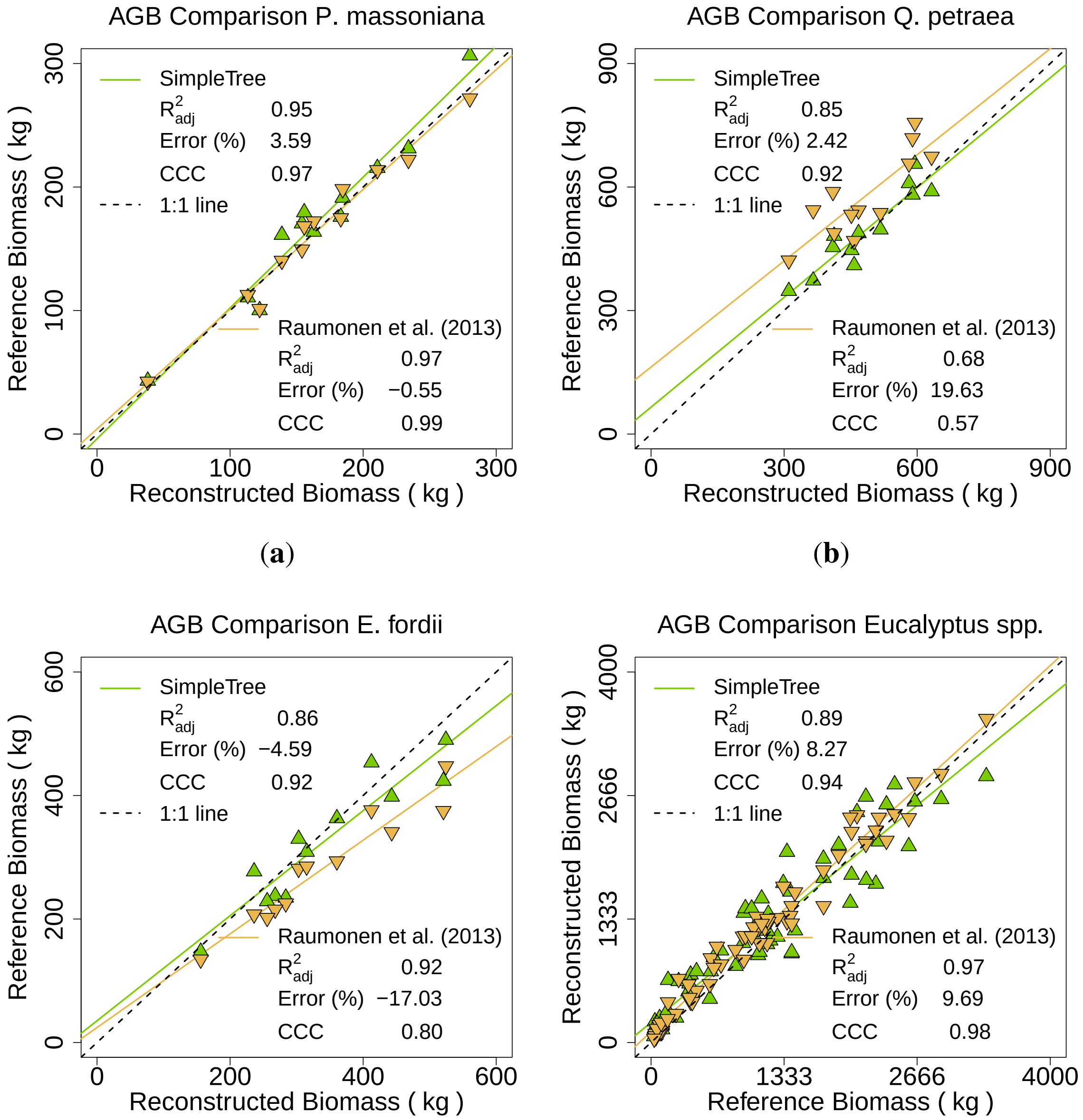

(**a**)

(**b**)

(**c**)

(**d**)

Figure 16. Comparison of two different QSM methods between ground truth AGB and TLS derived AGB of the species: **(a)** *P. massoniana*; **(b)** *Q. petraea*; **(c)** *E. fordii*; **(d)** *Eucalyptus spp.*

6. Discussion

Software SimpleTree implements a method capable of producing cylinder models that match field-measured estimates of volume and/or biomass to within ∼8% for all analysed tree species. While in Hackenberg *et al.* [10,12] only high resolution point clouds have been used as input data for this method, the utilization of *Eucalyptus spp.* data revealed the possibility to adapt this method to work on plot level scans.

Modelling twelve *Q. petraea* clouds (500,000 to 1,500,000 points per cloud) could be achieved within 10 min,which is a significant improvement from earlier works [12]. The average computation time per model for those clouds excluding stem point detection and visualization routines, but including cloud to model distance computation is ∼17 seconds on one core or ∼2.4 seconds with the multi-threaded approach on seven cores (numbers derived from **Parameter Optimization** analysis with more than 100,000 modelling runs of *Q. petraea*).

Hackenberg *et al.* [10] results showed, that the modelling of twigs can be problematic and might lead to an overestimation of AGB results for the complete tree. The **Allometric improvement** was introduced as a statistical improvement method to account for this problem. The average error for the *Q. petraea* models was reduced to 2% with this improvement, Hackenberg *et al.* [10] results showed here an ERROR_REL of 34%. Fitting an allometric function of the form of Equation (3) can also estimate the AGB of removed twigs, this can be observed for the *E. fordii* models.

Calders *et al.* [9] did propose the taper correction applied to the QSM models to achieve a similar effect. By including the **Allometric improvement** in the Raumonen *et al.* [49] code, a comparison between the taper and the allometric correction could be performed. For all three data sets, *i.e.*, *Q. petraea, P. massoniana* and *E. fordii* clouds, the comparison revealed that the allometric approach seems to be superior to the taper corrections. For *E. fordii* the additive component to estimate the removed twigs was not utilized in the Raumonen *et al.* [49] modelling, a further improvement of the results could be expected by implementing this function.

The automatic estimation for the minimum radius parameter in the **Allometric improvement** can still be problematic. For *Q. petraea* and *P. massoniana* clouds the minimum diameter was set to 0.5 cm in software SimpleTree, as here the cylinder models reached to the tip of twigs. The results proved this approach reasonable. In *E. fordii* clouds twig-points were removed during the de-noising procedures. A hard-coded threshold of 0.5 cm is therefore not desired. As the quality of the de-noised clouds representing the main branching structure of those trees is still considered high, the automatic search for this parameter was successful. In the *Eucalyptus spp.* clouds also twigs have been removed, but the cloud quality is poorer here. The point density is lower, noise points could not have been removed as efficiently and the double effect of small twigs due to imperfect co-registration of multiple scans was observed more often. Those reasons forced the optimization routine to find a minimum radius of 4 or 4.5 cm for the majority of trees. SimpleTree reconstructed results should in fact underestimate the ground truth volume for *Eucapytus spp.* due to the removal of twigs. We assume that the main reason in unexpected overestimation is an overestimated minimum radius.

Also problematic for *Eucalyptus spp.* is the fact, that for three species with different growth patterns only one allometric function was applied.

Utilizing the average euclidean cloud to model distance as an error term in parameter optimization seems to be beneficial for both for the SimpleTree software as well as for the Raumonen *et al.* [49] approach. In Calders *et al.* [9] parameters of QSM modelling have been optimized by visual inspection for completeness of the models. This user dependent decision was replaced by a fully automatic parameter search. As an automatic approach is considered superior to a supervised one in general, this is considered an improvement. The remaining problem in the minimum radius search for the allometric correction was already mentioned before.

Direct comparison between the Raumonen *et al.* [49] modelling and the SimpleTree software by utilizing the combined data set of all 101 trees reveals, that the CCC of the Raumonen *et al.* [49] approach is slightly higher (0.98 instead of 0.95). By a more detailed look utilizing each data set by itself it becomes clear, that both methods have their strengths. For *P. massoniana* both approaches resulted in a high CCC (Raumonen *et al.* [49] = 0.99 and SimpleTree = 0.98), the Raumonen *et al.* [49] results are slightly better. We consider the TLS reconstructed results for both approaches as highly accurate and the minor prediction errors for this species are already in the range of ground truth errors which have to be expected [94].

For *E. fordii* SimpleTree results have been more accurate (CCC of 0.92 instead of 0.80). The reason here might be partially in the usage of Equation (3) instead of Equation (1) in the SimpleTree software. Also the Raumonen *et al.* [49] approach without statistical radii correction resulted here in a higher CCC of 0.91 but was not used for comparison as it was desired to apply the same exact approach for all data sets.

For *Q. petraea* clouds SimpleTree results revealed a CCC of 0.92, while the Raumonen *et al.* [49] results showed a CCC of 0.57.

The *Eucalyptus spp.* scans revealed a slight superior CCC results for the Raumonen *et al.* [49] approach with a value of 0.98 instead of 0.94 for the SimpleTree results.

It should here be mentioned, that *E. fordii*, *P. massoniana* and *Q. petraea* scans were already used in Hackenberg *et al.* [10] utilizing the **Sphere Following** method, while the *Eucalyptus spp.* data set was used for QSM [49] modelling in Calders *et al.* [9].

The following comparisons to other methods are made for general guidance only; they use different data from those used here, and the reconstruction methods rely on different assumptions. As a result the direct comparison with the method of Raumonen *et al.* [49] should be considered the only truly direct result.

Belton *et al.* [47] utilized a single reconstructed tree model to validate the volume estimates of their method. The comparison of the reconstructed volume and mass to the results of an allometric function leads to an ERROR_REL of ∼117%. However, allometric functions potentially contain large and unquantified errors. Calders *et al.* [9] show this in relation to destructive measurements and compared to lidar-derived QSMs. The target tree used by Belton *et al.* [47] is larger than any tree used here. The pure magnitude of the error indicates that SimpleTree models tend to be more accurate. However, until the same point clouds are analysed by the different methods, direct accuracy comparisons cannot be established. We note that the proposed de-noising procedure in the work of Belton *et al.* [47] may be preferable to that used in SimpleTree, as it does not require manual interaction.

Dassot *et al.* [13] reported an ERROR_REL of ∼10% for the stem predictions and ∼30% for the branch prediction of 42 processed trees. The unreported ERROR_REL of total AGB volume therefore has to be between this values, but is considered to be near ∼10%, as branches only contribute minor to total AGB. The ERROR_REL of SimpleTree results for the combined data set for total AGB is described with a value of 7.24%. Therefore SimpleTree results seem to be more accurate than the one of Dassot *et al.* [13]. The SimpleTree method also does not rely on manual interaction after preliminary threshold adjustment.

Kankare *et al.* [14] achieved an Root Mean Squared Error (RMSE) of 12.93% and 11.90% on AGB estimations of a data set containing two coniferous tree species—no Akaike information criterion given here [95,96]. The correlation coefficients of 0.95 and 0.98 correspond to R^2 values of 0.96 and 0.90, with smaller expected $R^2_{adj.}$ values. The RMSE cannot be transformed to the here utilized ERROR_REL. On coniferous trees SimpleTree results reveal the highest correlation to the destructive biomass estimators, indicated by an $R^2_{adj.}$ value of 0.95 and an error of less than 4%. As the SimpleTree reconstruction method works best on coniferous trees, the software might be better suitable for AGB predictions, but the accuracy benefit is considered minor. Regarding the combined data set results it appears that both methods are quite accurate, *i.e.*, mostly agree $\leq$ 10% error. Besides not relying on manual measurements for feature extraction the SimpleTree software also has the additional benefits of being open source and implementing a QSM method. These two points are discussed briefly in the following section.

6.1. The Benefit of Open Source

The Computree [70] platform is written in C++ and supports PCL usage. Due to the strict modularization, efficient integration of other methods is possible. In fact, while not being considered stable yet, the Spherefollowing routine of SimpleTree was isolated from the user interface and could be integrated in the Computree platform. One of the strength of available Computree modules is the automatic segmentation of plot level scans into isolated tree clouds. Those isolated clouds can be further processed with the SimpleTree algorithm, as can be seen in Figure 17.

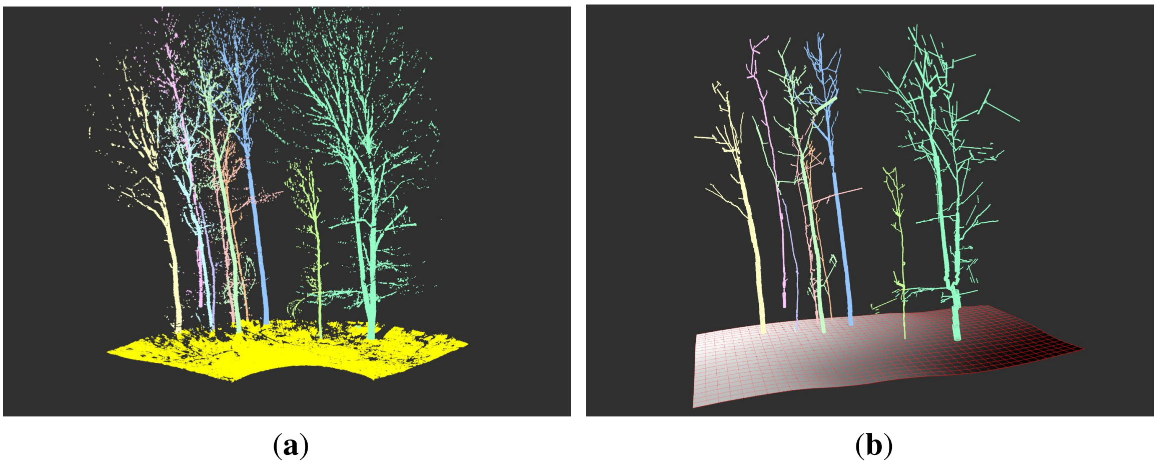

Figure 17. A visual output of the SimpleTree algorithm within the Computree platform.

On the left picture the segmentation of a single scan mode point cloud with heavy occlusion is depicted. The segmentation was performed with Computree core functionalities into ground cloud and individual tree clouds. From the ground cloud a DTM was generated with another core functionality of Computree, while from the tree clouds SimpleTree cylinder models were created. Such a symbioses reduces the amount a single scientist has to perform by itself.

6.2. The Benefit of QSMs

Besides accurate AGB estimations QSMs can give answers to several forestry relevant questions. This section is meant to give some applied examples performed on a single test model of a *Prunus avium*. These results should be seen as preliminary results not meant to be used in other works before deeper analysis is performed on a larger amount of trees.

Stem curves can be extracted efficiently from the results models, as can be seen in Figure 18. This stem curve is not validated on ground truth data, but shows a strong natural pattern.

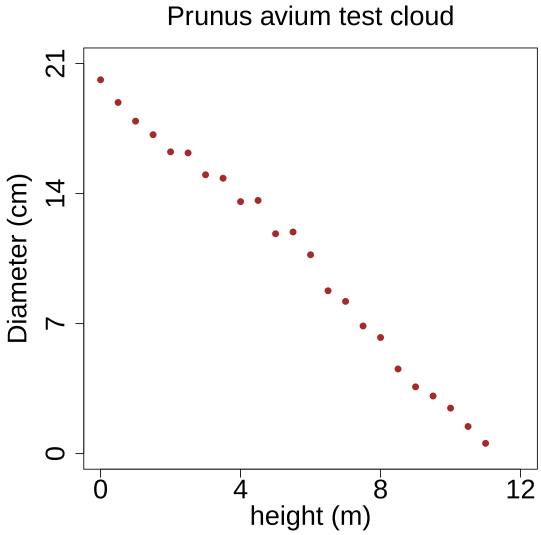

Figure 18. Stem curve of a *Prunus avium.*

Additionally the branches of the same target tree have been binned according to the height of their base. The utilized bin width here is half a meter, within a bin the volume of all contained branches was summed up. In Figure 19 only three major whorls are visible, the height of the first whirl can be defined as the crown base.

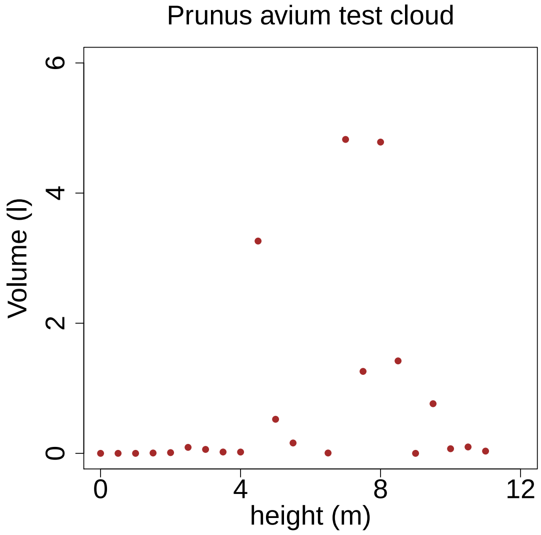

Figure 19. Branch volume distribution in height bins of the stem of a *Prunus avium.*

The method of Côté *et al.* [42] relies on the pipe model theory [43]. This theory states, that the cross sectional area before a branch junction equals the sum of the cross sectional areas after the branch junction. We converted the median radii of segments into cross sectional areas. In Figure 20 the cross sectional area of parent segments is plotted against the sum of areas of the child segments. The fitted linear model has only a slope of 0.944. This can be seen as an indicator, that the pipe model theory has to be adjusted with nowadays superior methods.

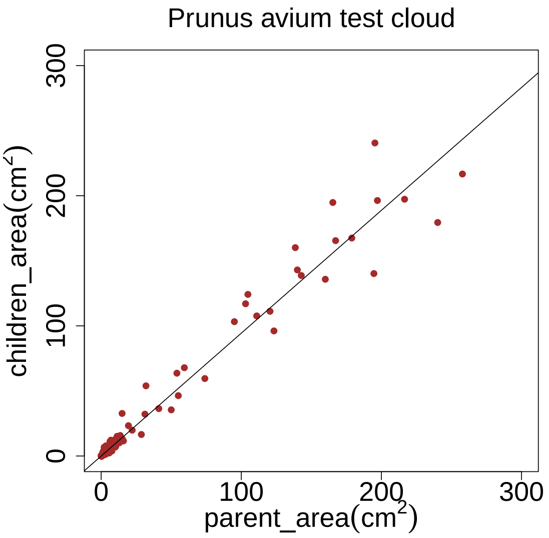

Figure 20. Improvement possibilities of the pipe model theory [43] with a *Prunus avium* model.

A time series analysis utilizing SimpleTree is in preparation by Sheppard *et al.* [97]. Clouds of several *Prunus avium* were transformed into the same coordinate system with the ICP functionality. Several thousand segment pairs of the resulting QSMs from different years have been matched according to their spatial distance. In Figure 21 the median diameter of those matched segments is depicted. The color red refers to a bad match, while the color green is considered a good match. The good matches show a clear increasing trend, quantification and discussion are performed in Sheppard *et al.* [97].

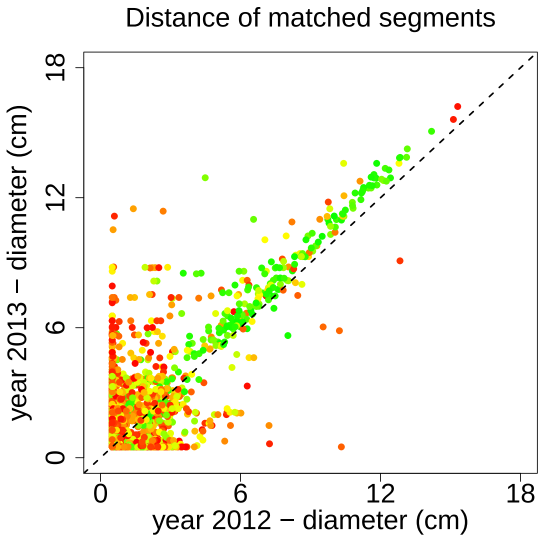

Figure 21. Time series analysis of several *Prunus avium*.

7. Outlook

The state of the art reveals two different kind of methods. Some aim to be more robust and independent to user input. The proposed method on the other hand is more sensitive to user chosen parameters. The analysis section reveals that the optimization of an input parameter set results in a larger accuracy of the cylinder models. We assume, such high quality of models cannot be derived from less sensitive methods.

Bad input parameters though lead to undesirable models. We conclude that the most beneficial way to estimate high accurate models is to create an artificial intelligence (AI) to support the threshold setting for sensitive methods like ours.

The proposed optimization method is a brute force one. Literature reports optimization algorithms such as the downhill simplex method published in Nelder *et al.* [98] or other methods described in Press *et al.* [99]. Libraries like Scipy [100] provide implementations of those methods. While a library gives the freedom to test a wide range of robust algorithm implementations in a short time frame, the library usage also adds more dependencies to a software. More dependencies lead to difficulties in distributing the software and therefore the authors decided against the usage of Scipy.

Yet it is envisaged to include stable implementations of peer-reviewed optimization methods in future releases. Furthermore, initial starting parameters sets should be created from human readable questions, e.g. questions referring to tree species or scanning resolution. Tree species detection by itself can be implemented in the software, reducing the amount of user input further. Results of Othmani *et al.* [32] relying on feature extraction of the bark structure classified with Random Forest [101] can be used for further development in classification.

With such approaches even parameter sensitive methods can give more user independent results, as parameter choice is supported by the AI. Therefore high accuracy tree models can be developed also by users not familiar with the underlying algorithms.

8. Conclusions

Software SimpleTree implements a tree modelling method, which is considered highly accurate as it was used to predict the above ground biomass for six different species with an average relative error of $\leq 8\%$ and a concordance correlation coefficient of $>=$0.92 for each data set. The implementation is fast, allowing users to build large data processing pipelines for many trees, which can be run efficiently and within a few hours or days.

The public availability of the source code allows the recompilation of the program on different Operating Systems with a C++ compiler. The recommended system for using SimpleTree is Ubuntu Linux, but it has also been successfully compiled on Windows 7. This assures the possibility to use this software tool even in the future, where additional improvements and contributions and modifications from other users can be easily incorporated, as desired.

First steps to automatically estimate sensitive input parameters have already been implemented to automize the approach further. This is especially important when modelling a large number of trees.

The Raumonen *et al.* [49] method and the SimpleTree software are utilizing two different algorithms. As the results from those two methods are comparable to each other, terrestrial laser scanning clouds can be viewed as an accurate measurement tool to record the volume distribution of above ground biomass of trees.

Acknowledgments

The research was funded by the Federal Ministry of Education and Research (BMBF) within the Lin2Value project (support code 033L049A).

The article processing charge was funded by the German Research Foundation (DFG) and the Albert Ludwigs University Freiburg in the funding programme Open Access Publishing.

The Eucalyptus forest inventory and destructive sampling data are owned by The University of Melbourne, Department of Forest and Ecosystem Science, Water St., Creswick, Victoria 3363, Australia (Contact either Simon Murphy or Chris Weston: murphys@unimelb.edu.au; weston@unimelb.edu.au).

The authors would like to express their thanks to Elena Roßkopf, Georgios Skiadaresis and Raphael Ehnis for preprocessing point cloud data. To Christopher Morhart for guiding the software development to forestry relevant research questions and to Martin Mann and Andreas Hamann for general support in contributing to the open domain. A special thanks goes to Kathy Chiu, Marc Wassenberg and Stephan Hoffmann for their contribution in the destructive harvesting of the trees during Lin2Value field work.

We also want to give appropriate credit to the core developer team of the PCL, namely Victor Lamoine, Sergey Alexandrov and Jochen Sprickenhof, as well as to the core developer team of Computree, namely Alexandre Piboule and Michael Krebs.

The quality of the presented manuscript did improve significantly during the revision based on the feedback of the four unknown reviewers. Our final thank is addressed to the academical editors for stating out the relevance of the comparison of SimpleTree results to other methods.

Author Contributions

The contribution of the authors to this work is as stated:

Jan Hackenberg developed and implemented the sphere following method of Software SimpleTree, as well as other discussed functionalities. The user interface as well as the homepage, which gives support information, was fully developed by him. Except external data preparation all SimpleTree results have been produced by Jan Hackenberg.

Both allometric improvement and parameter optimization were developed in majority by Jan Hackenberg, while during development process Mathias Disney, Kim Calders and Pasi Raumonen contributed as well by discussing those approaches. Pasi Raumonen took full responsibility to implement these methods as well in his software.

The QSM approach was developed by Pasi Raumonen and all QSM results have been produced by him and Kim Calders. He is responsible for implementing the parameter search and allometric improvement in the QSM code.

The manuscript preparation was performed by Jan Hackenberg, Pasi Raumonen, Mathias Disney and Kim Calders. All authors participated in the review process.

Heinrich Spiecker takes credit to support the software development of SimpleTree as the project coordinator of the Lin2Value project. He additionally guided the algorithm improvement of Software SimpleTree to produce forestry relevant output data.

Conflicts of Interest

The authors declare no conflict of interest.

Appendix

A. De-noising

E. fordii

A fully automatic method to de-noise the scans was implemented, though showing losses in the crown structure. First, a **Voxel-Grid Filter** (0.005) was applied to the input cloud. Afterwards an intensity histogram was computed. All points with an intensity larger the histogram maximum plus a user-defined threshold (15) were deleted. With the **Curvature Outlier Removal** (0,55,0,100,0,100) more needle hits were removed. With a **Conditional Outlier Removal** (30, 4) isolated points were removed. By **Euclidean Clustering** (0.02) procedure the tree was separated from remaining artefacts. The whole procedure took 16.5 min for all twelve trees.

A second manual de-noised data set was created in two hours of work. Only **Intensity Outlier Removal** (∼110, 255), **Euclidean Clustering** (∼0.02) and the **Crop Sphere** (0.2–1) were used.

P. massoniana

The automatic filtering routine consists of the following steps:

First the cloud size was reduced with a **Voxel Grid Filtering** (0.005). Then needle hits were reduced with the **Curvature Outlier Removal** (0, 45, 55, 100, 0, 45) The two last steps were a **Statistical Outlier Removal** (30, 0.9) and an **Euclidean Clustering** (0.02) routine. Running this pipeline took 42 min for all trees. Some large artefacts of other trees remained in the cloud. More automatic removal of noise points has resulted in an unacceptable loss of biomass information.

An additional manual removal of the artefacts was performed in 30 min by using **Crop Spheres** (0.1–1) and **Euclidean Clustering** (0.02) on the automatic output.

Q. petraea

Noise was reduced by the following fully automatic pipeline:

First data size was reduced by a **Voxel Grid Filter** (0.005). Afterwards a **Statistical Outlier Removal** (30, 0.5) was performed, followed by an **Euclidean Clustering** (0.02). The last two steps were repeated one time to further reduce the noise. The complete de-noising took 28.6 min for all trees.

An additional manual removal of the artefacts was performed in 30 min by using **Crop Spheres** (0.1-1) and **Euclidean Clustering** (0.02) on the automatic output.

Eucalyptus leucoxylon, Eucalyptus microcarpa and Eucalyptus tricarpa

Here the **Curvature Outlier Removal** (0, 55, 0, 100, 0, 100) was used in a first step, followed by an **Euclidean Clustering** (0.06–0.12). Remaining leaf artefacts were manually deleted with **Crop Spheres** (0.1–1). The procedure took two hours for all 65 clouds.

B. Result tables

Table B1. Results for *Q. petraea*.

ID	$\mathbf{AGB}_{\text{GT}}$ (kg)	$\mathbf{AGB}_{\text{Hackenberg } et\ al.}$ (kg)	$\mathbf{AGB}_{\text{Raumonen } et\ al.}$ (kg)
Q1	458	410	469
Q2	311	347	422
Q3	595	656	756
Q4	518	497	537
Q5	413	481	488
Q6	468	488	543
Q7	366	373	544
Q8	633	589	674
Q9	582	609	657
Q10	412	453	588
Q11	452	447	533
Q12	590	581	719

Table B2. Results for *E. fordii*.

ID	$\mathbf{AGB}_{\text{GT}}$ (kg)	$\mathbf{AGB}_{\text{Hackenberg } et\ al.}$ (kg)	$\mathbf{AGB}_{\text{Raumonen } et\ al.}$ (kg)
E1	284	234	225
E2	236	277	207
E3	268	237	215
E4	303	330	281
E5	521	424	375
E6	156	147	134
E7	256	229	202
E8	412	453	376
E9	443	398	341
E10	524	490	447
E11	361	363	293
E12	315	309	285

Table B3. Results for *P. massoniana*.

ID	$\mathbf{AGB}_{\text{GT}}$ (kg)	$\mathbf{AGB}_{\text{Hackenberg } et\ al.}$ (kg)	$\mathbf{AGB}_{\text{Raumonen } et\ al.}$ (kg)
P1	280	306	272
P2	113	111	113
P3	154	170	149
P4	139	161	140
P5	185	191	198
P6	211	215	214
P7	163	164	172
P8	38	43	42
P9	156	179	168
P10	183	176	175
P11	234	231	222
P12	122	100	101

C. Abbreviations

Table C1. List of *Parameters*

AGB	**A**bove **G**round **B**iomass
AI	**A**rtificial **I**intelligence
ALS	**A**irborne **L**aser **S**canning
CCC	**C**oncordance **C**orrelation **C**oefficient
CO$_2$	**C**arbon di**o**xide
DBH	**D**iameter at **B**reast **H**eight
DBSCAN	**D**ensity **B**ased **S**patial **C**lustering of **A**pplications with **N**oise
DTM	**D**igital **T**errain **M**odel
ERROR_REL	total **REL**ative - **ERROR**
FIFO	**F**irst **I**n - **F**irst **O**ut (queue)
ICP	**I**terative **C**losest **P**oint
LiDAR	**Li**ght **D**etection **A**nd **R**anging
NLS	**N**on-linear **L**east **S**quares
PCA	**P**rincipal **C**omponent **A**nalysis
QSM	**Q**uantitative **S**tructural tree **M**odels
RANSAC	**Ran**dom **Sa**mple **C**onsensus
RMSE	**R**oot **M**ean **S**quared **E**rror
TLS	**T**errestrial **L**aser **S**canning
VLS	**V**ehicle-based **L**aser **S**canning

Table C2. List of *Parameters*

	Radius Outlier Removal
r	the radius for the ϵ-neighbourhood search
k	the minimum number of points in range r
	Statistical Outlier Removal
k	the number of nearest neighbours used for computing mean and standard deviation of distances
sdMult	the standard deviation is multiplied by this factor and added and subtracted from the mean for a range
	Voxel Grid Filtering
cellsize	the cell-size of a voxel in which all points are merged
	Curvature Filtering
minX/maxX	range parameter for the eigenvalue λ_X
	Intensity Filtering
min/max	range parameter for the intensity

Table C2. *Cont.*

	Crop Sphere
radius	the radius of the deletion sphere
	Euclidean Clustering
clusterTolerance	the minimum distance between two clusters
minPts	the minimum number of contained points for a cluster creation
numCluster	the maximum number of returned clusters
	Euclidean Clustering
sphereMultiplier	the factor of enlargement in the circle to sphere transformation
epsClusterStem	the cluster tolerance for stem points
epsClusterBranch	the cluster tolerance for branch points
epsSphere	the search size around the sphere surface
minPtsRansacStem	the minimum number of stem points for RANSAC fit
minPtsRansacBranch	the minimum number of branch points for RANSAC fit
minPtsClusterStem	the minimum cluster size for stem points
minPtsClusterBranch	the minimum cluster size for branch points
minRadiusSphereStem	the minimum radius for a sphere build from stem points
minRadiusSphereBranch	the minimum radius for a sphere build from branch points
	Allometric Improvement
a	parameter of NLS fit
b	parameter of NLS fit
fac	a is divided by fac for a minimum radius value computation
minRad	the minimum radius of a cylinder after the improvement
	Parameter Optimization
iterations	the maximum number of iterations
criterion	the minimum improvement for a new iteration to start
seeds	the number of random seeds of parameter sets per iterations
	Crown Computation
α	parameter for α-shape computation
	Iterative Closest Point
β	the rotation angle for the alignment of two clouds

D. Sphere Following Routine

Cutting sphere surfaces with a tree point cloud to detect circular structures was already utilized in Jayaratna [66]. The presented algorithm is build on this idea.

A sphere with its center point located on the skeleton of a tree and with a radius larger than the underlying branch segment is used to extract a sub point cloud P_{sub} located on the sphere surface. If the sphere is not located at the tip of the branch, the sub point will represent a cross sectional area of the underlying branch segment. The cross sectional area is a circular structure, see Figure C1.

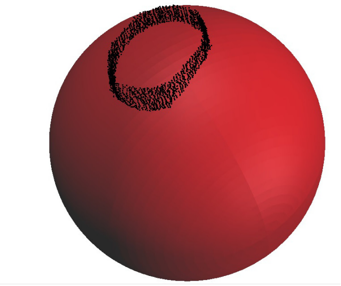

Figure C1. A sphere utilized by the cylinder fitting routine extracting a sub point cloud on the sphere surface (figure taken from Hackenberg *et al.* [12]).

Into the sub point cloud a circle is fitted with random sample consensus (RANSAC) routine [85]. The sphere center is utilized as a start point for a finite cylinder, the circle center point serves as the end point and the circle radius as the cylinder radius, see Figure C2.

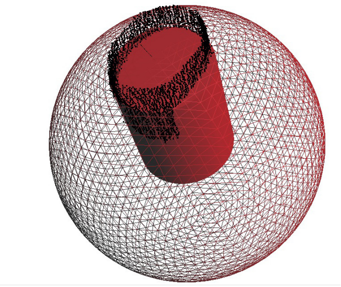

Figure C2. The fitted circle is used to generate a finite cylinder (figure taken from Hackenberg *et al.* [12]).

If the circle is transformed to a three dimensional sphere including an enlargement of its radius, the procedure can be repeated recursively, depicted in Figure C3. During the processing of one sphere all points from the input cloud contained in the sphere are removed to prevent the algorithm from jumping back and forth infinitely.

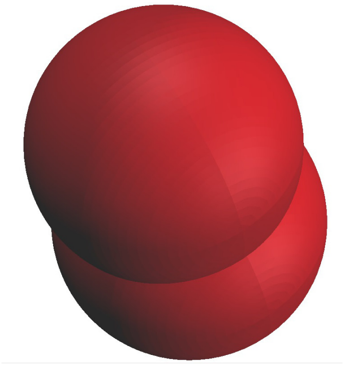

Figure C3. The circle is transformed to a sphere and the procedure is repeated (figure taken from Hackenberg *et al.* [12]).

The method as described needs to be extended to process branch-junctions successfully. In branch junctions multiple cross sectional areas are included in P_{sub}. P_{sub} needs to be clustered according to the segmentation and spatial distance of points into clusters P_i. If zero clusters are found, the algorithm reached the tip of a branch and the recursion ends. If exactly one cluster is found, the above description works as proposed. In case multiple clusters are found, into each P_i a circle is fitted, see Figure C4.

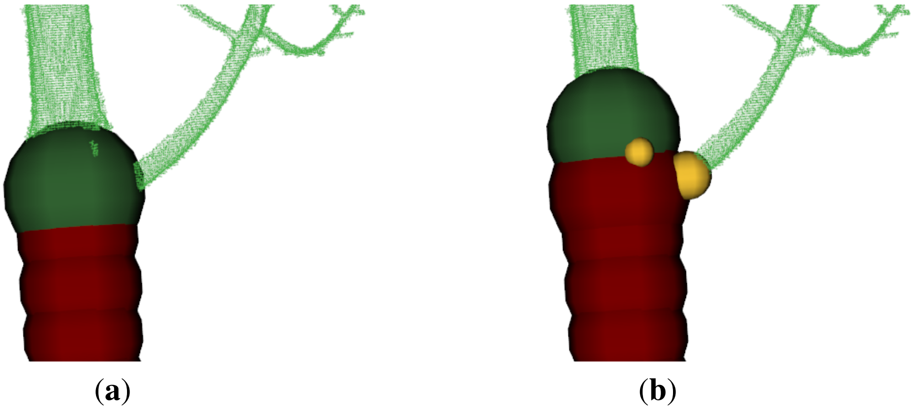

Figure C4. The sphere-following algorithm reaches a branch junction: **(a)** multiple clusters are located on the sphere surface; **(b)**into each cluster a circle is fitted and transformed to a sphere.

The largest fitted circle/sphere is processed first (marked green in Figure C4 (b)), the other spheres (colourized in yellow) are stored in a First In-First Out (FIFO) queue to be processed later. When a sphere reaches a branch's tip and no more clusters can be found on the sphere-surface, the first member of the FIFO queue is processed and removed from the queue. The algorithm is initialized by fitting a circle into the cluster with lowest z-coordinate of the de-noised cloud.

The algorithm is supposed to follow the stem first, already detecting the bases of first order branches along its path. After reaching the stem tip, the first sphere stored in the FIFO queue is processed, see Figure C5 (a).

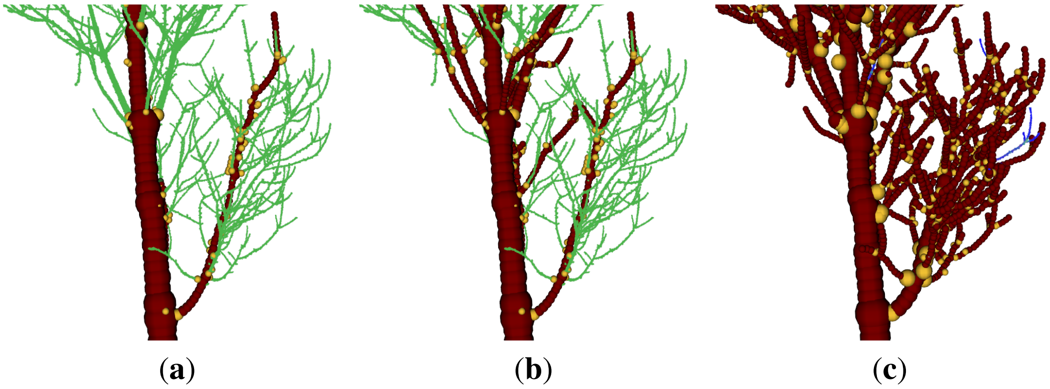

Figure C5. The algorithm processes different branch orders separately.

During the processing of this first order branch, the bases of second order branches are already detected and stored in the FIFO queue. When reaching the tip of the processed first order branch, the next first order branch is processed. The detected second order branches are processed after the last first order branch (Figure C5 (b), (c)). The algorithm terminates when the FIFO queue is empty while a processed branch reaches its tip.

D.1. Post Processing

The first detected cylinder serves as the root of the tree model. For all other cylinders the cylinder's start point equals the end point of another cylinder. This fact enables the storage of the cylinders in an efficient informatics tree structure. A cylinder, whose end point equals the start point of a second cylinder, is considered to be the parent of this second cylinder and the second cylinder is named child of the first one.

With the root cylinder, which is stored in the root node, an iterative search starts to build the tree structure. For each processed cylinder all children are looked up. If the cylinder has only one child, this child is stored in the same node. If a cylinder has multiple children, for each child a new node connected to the parent node is generated. If no children are found the tree structure ends in a leaf node. Multiple cylinders stored in one node are called segments and are stored in an ordered list. As soon as a child cylinder is added to the structure, it is processed like its parent, *i.e.*, it's children are added to the structure as well.

A segment in the storage structure relates to the part of a branch between two neighbouring branch junctions of the modeled tree. Several post processing procedures can be performed utilizing this structure.

In Figure C6 shoots are depicted near the stem. The shoots grow parallel to the stem in a small distance to the stem. The spheres utilized in detecting the stem are large and so multiple successive stem spheres intersect with points representing the same shoot. Every sphere, whose surface intersects with the points of this shoot, results in a cylinder connecting stem and shoot.

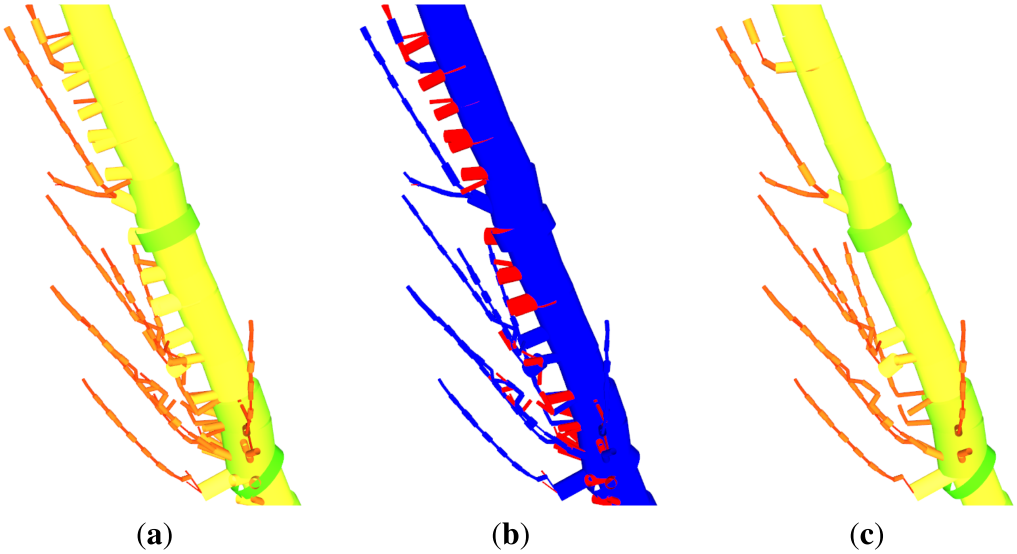

Figure C6. Post processing—removal of wrong connection cylinders between two different segments.

Only the first cylinder connecting the stem to the shoot is desired. As this cylinder is detected first by the algorithm, due to the nature of the FIFO queue, it is also processed first. At the time the other cylinders are processed (or more accurately spoken the stored spheres from which the cylinders are build), the whole shoot has already been followed and the points representing the shoot are removed. Therefore no child cylinders are generated for those cylinders. In the tree structure those cylinders are stored in leaf nodes. These leaf nodes contain only one cylinder. All segments stored in leaf nodes containing only one cylinder (coloured red in Figure C6 (b)) are removed from the structure (Figure C6 (c)). Leaf nodes representing tips of branches tend to have more than one cylinder and are not affected by this procedure.

Afterwards in each remaining segment two successive cylinders are merged into one if possible. The merged cylinders' radii are averaged. In Figure C7 it can be seen that the cylinders' axes and radii are smoothed by this procedure. Also more points can be allocated to a single cylinder after the merge operation, stabilizing the fit improvement occurring later in the post-processing procedures.

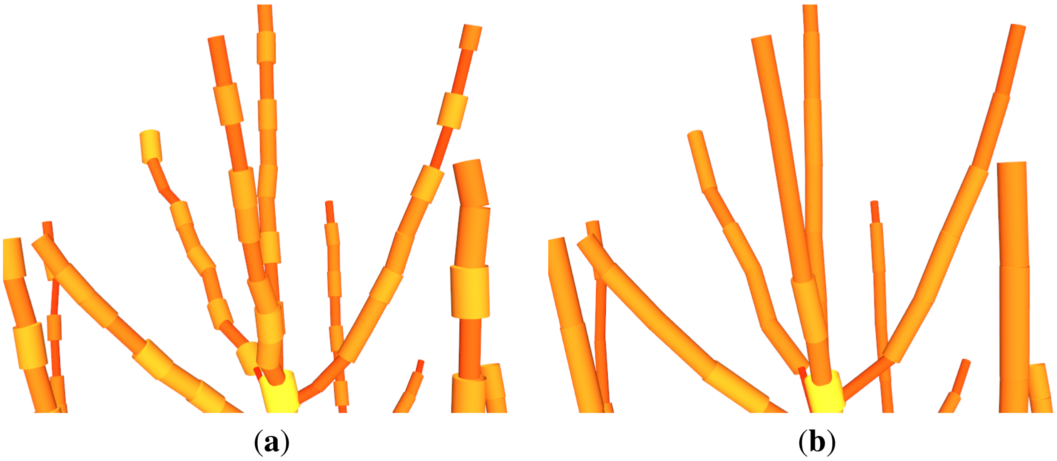

Figure C7. Merging of successive cylinders : **(a)** before the merge operation; **(b)** after the merge operation.

The axis of the first cylinder of a segment is often poorly aligned with the underlying branch axis. Therefore the start point of the first cylinder of the axis is projected to the infinite axis of the second cylinder. The result of this improvement is depicted in Figure C8.

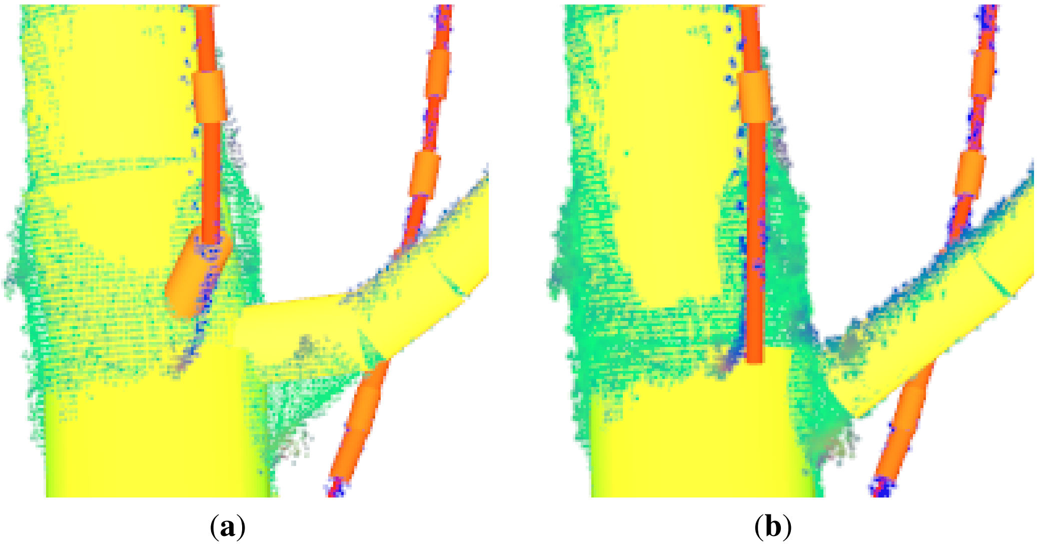

Figure C8. Merging of successive cylinders : **(a)** before the merge operation; **(b)** after the merge operation.

Until now only circle fitting but no cylinder fitting has been performed. The detected cylinders though are a good representation of the underlying branching structure. Points near the preliminary detected cylinders are allocated to the cylinders. After the allocation a RANSAC cylinder fitting is performed if the majority of the allocated points are stem points or the median method proposed in Hackenberg *et al.* [12] otherwise. Although the former utilized NLS cylinder fit was replaced by the RANSAC routine the arguments to use the median method for twigs still hold true. With threshold adjustment the user of SimpleTree can influence the usage of the two methods, but this is out of the scope of this summary. The result of this post processing procedure is depicted in Figure C9.

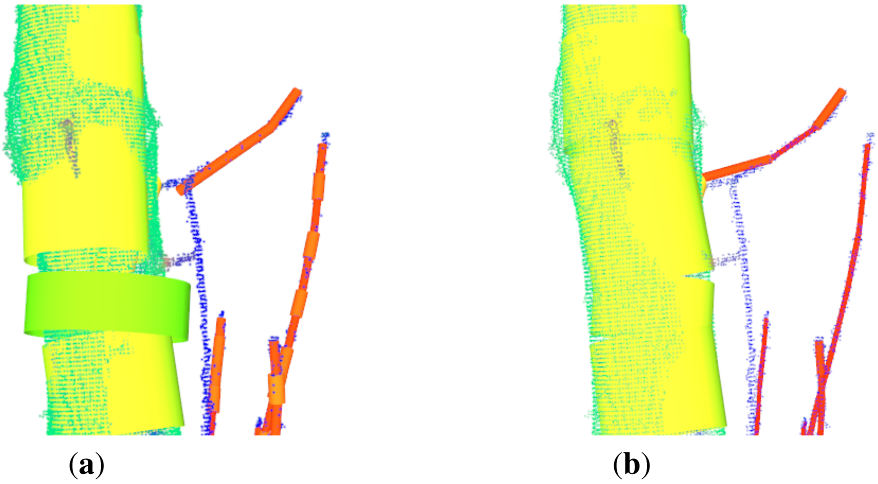

Figure C9. The effect of the cylinder fitting improvement : **(a)** one cylinder of the stem is bad fitted before the improvement; **(b)** the same cylinder represents the stem form better after the improvement.

If despite the usage of the median method overestimated cylinders occur, their radii are adjusted. If a cylinder's radius is larger than 120% (or smaller than 80%) of the segments median radius it's radius is set to the median radius, see an example in Figure C10.

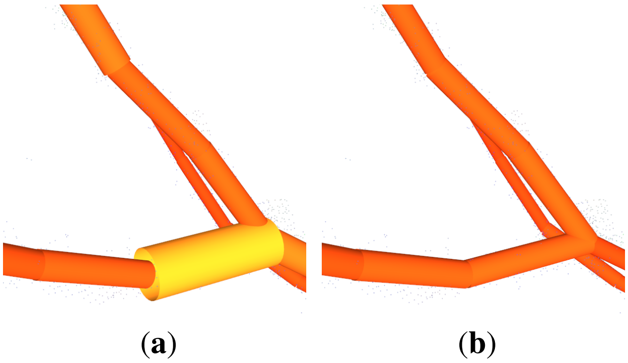

Figure C10. The effect of the radius median segment check : **(a)** one cylinder of a branch is overestimated before the improvement; **(b)** the cylinder's radius is set to the median radius of it's segment.

References

1. Simonse, M.; Aschoff, T.; Spiecker, H.; Thies, M. Automatic determination of forest inventory parameters using terrestrial laser scanning. In Proceedings of the ScandLaser Scientific Workshop on Airborne Laser Scanning of Forests, Umea, Sweden, 19 September 2003; pp. 252–258.
2. Thies, M.; Pfeifer, N.; Winterhalder, D.; Gorte, B.G. Three-dimensional reconstruction of stems for assessment of taper, sweep and lean based on laser scanning of standing trees. *Scand. J. For. Res.* **2004**, *19*, 571–581.
3. Hopkinson, C.; Chasmer, L.; Young-Pow, C.; Treitz, P. Assessing forest metrics with a ground-based scanning lidar. *Can. J. For. Res.* **2004**, *34*, 573–583.
4. Pfeifer, N.; Gorte, B.; Winterhalder D. Automatic reconstruction of single trees from terrestrial laser scanner data. *Int. Arch. Photogram. Rem. Sens. Spat. Inform. Sci.* 2004, *35*, 114–119.
5. Leeuwen, M.; Nieuwenhuis, M. Retrieval of forest structural parameters using LiDAR remote sensing. *Eur. J. For. Res.* **2010**, *129*, 749–770.
6. Dassot, M.; Constant, T.; Fournier, M. The use of terrestrial LiDAR technology in forest science: Application fields, benefits and challenges. *Ann. For. Sci.* **2011**, *68*, 959–974.
7. Newnham, G.J.; Armston, J.D.; Calders, K.; Disney, M.; Lovell, J.L.; Schaaf, C.B.; Strahler, A.H.; Danson, F.M. Terrestrial laser scanning for plot-scale forest measurement. *Curr. For. Rep.* **2015**, *1*, 239–251.
8. Kaasalainen, S.; Krooks, A.; Liski, J.; Raumonen, P.; Kaartinen, H.; Kaasalainen, M.; Puttonen, E.; Anttila, K.; Mäkipää, R. Change detection of tree biomass with terrestrial laser scanning and quantitative structure modelling. *Remote Sens.* **2014**, *6*, 3906–3922.
9. Calders, K.; Newnham, G.; Burt, A.; Murphy, S.; Raumonen, P.; Herold, M.; Culvenor, D.; Avitabile, V.; Disney, M.; Armstong, J.; *et al.* Nondestructive estimates of above-ground biomass using terrestrial laser scanning. *Methods Ecol. Evol.* **2015**, *6*, 198–208.
10. Hackenberg, J.; Wassenberg, M.; Spiecker, H.; Sun D. Non destructive method for biomass prediction combining TLS derived tree volume and wood density. *Forests* **2015**, *6*, 1274–1300.
11. Raumonen, P.; Casella, E.; Calders, K.; Murphy, S.; Åkerblom, M.; Kaasalainen, M. Massive-scale tree modelling from TLS data. *ISPRS Ann.* **2015**, 189–196, doi:10.5194.
12. Hackenberg, J.; Morhart, C.; Sheppard, J.; Spiecker, H.; Disney, M. Highly accurate tree models derived from terrestrial laser scan data: A method description. *Forests* **2014**, *5*, 1069–1105.
13. Dassot, M.; Colin, A.; Santenoise, P.; Fournier, M.; Constant, T. Terrestrial laser scanning for measuring the solid wood volume, including branches, of adult standing trees in the forest environment. *Comput. Electron. Agric.* **2012**, *89*, 86–93.
14. Kankare, V.; Holopainen, M.; Vastaranta, M.; Puttonen, E.; Yu, X.; Hyyppä, J.; Vaaja, M.; Hyyppä, H.; Alho, P. Individual tree biomass estimation using terrestrial laser scanning. *ISPRS J. Photogramm. Remote Sens.* **2013**, *75*, 64–75.
15. Van Laar, A.; Akça, A. *Forest Mensuration*; Springer London, Limited: London, UK, 2007; Volume 13.
16. Stallman, R. M. *Free Software, Free Society: Selected Essays of Richard M. Stallman*; Free Software Foundation, Boston, MA, USA. 2002.

17. Voegtle, T.; Schwab, I.; Landes, T. Influences of different materials on the measurements of a terrestrial laser scanner (TLS). *ISPRS2008* **2008**, *37*, 1061–1066.
18. Pesci, A.; Teza, G. Effects of surface irregularities on intensity data from laser scanning: An experimental approach. *Ann. Geophys.* **2008**, *51*, 839–848.
19. Pueschel, P.; Newnham, G.; Rock, G.; Udelhoven, T.; Werner, W.; Hill, J. The influence of scan mode and circle fitting on tree stem detection, stem diameter and volume extraction from terrestrial laser scans. *ISPRS J. Photogramm. Remote Sens.* **2013**, *77*, 44–56.
20. Pueschel, P. The influence of scanner parameters on the extraction of tree metrics from FARO Photon 120 terrestrial laser scans. *ISPRS J. Photogramm. Remote Sens.* **2013**, *78*, 58–68.
21. Rusinkiewicz, S.; Levoy; M. Efficient variants of the ICP algorithm. In Proceedings of the Third International Conference on 3-D Digital Imaging and Modeling, Quebec, Canada, 28 May–1 June 2001; pp. 145–152.
22. Hilker, T.; Coops; N.C.; Culvenor, D.S.; Newnham, G.; Wulder, M.A.; Bater, C.W.; Siggins, A. A simple technique for co-registration of terrestrial LiDAR observations for forestry applications. *Remote Sens. Lett.* **2013**, *3*, 239–247.
23. Lin, Y.; Jaakkola,, A.; Hyyppä, J.; Kaartinen, H. From TLS to VLS: Biomass Estimation at Individual Tree Level. *Remote Sens.* **2010**, *2*, 1864–1879.
24. Rutzinger, M.; Pratihast, A.K.; Elberink, O.; Sander, J.; Vosselman, G.. Tree modelling from mobile laser scanning data-sets. *Photogramm. Rec.* **2011**, *26/135*, 361–372.
25. Yao, T.; Yang, X.; Zhao, F.; Wang, Z.; Zhang, Q.; Jupp, D.; Lovell, J.; Culvenor, D.; Newnham, G.; Ni-Meister, W.; *et al.* Measuring forest structure and biomass in New England forest stands using Echidna ground-based lidar. *Remote Sens. Environ.* **2011**, *115*, 2965–2974.
26. Litkey, P.; Hyyppä, J.; Kaartinen, H.; Vastaranta, M.; Holopainen, M. Automatic Stem Mapping Using Single-Scan Terrestrial Laser Scanning. *IEEE Trans. Geosci. Remote Sens.* **2012**, *50*, 661–670 .
27. Liang, X.; Hyyppä, J.; Kaartinen, H.; Holopainen, M.; Melkas, T. Detecting changes in forest structure over time with bi-temporal terrestrial laser scanning data. *ISPRS Int. J. Geoinf.* **2012**, *1*, 242–255.
28. Yang, X.; Strahler, A.H.; Schaaf, C.B.; Jupp, D.L.B.; Yao, T.; Zhao, F.; Wang, Z.; Culvenor, D.S.; Newnham G.J.; Lovell, J.L.; *et al.* Three-dimensional forest reconstruction and structural parameter retrievals using a terrestrial full-waveform lidar instrument (Echidna). *Remote Sens. Environ.* **2013**, *7*, 36–51.
29. Srinivasan, S.; Popescu, S.C.; Eriksson, M.; Sheridan, R.D.; Ku, N.-W. Multi-temporal terrestrial laser scanning for modeling tree biomass change. *For. Ecol. Manag.* **2014**, *318*, 304–317.
30. Srinivasan, S.; Popescu, S.C.; Eriksson, M.; Sheridan, R.D.; Ku, N.-W. Terrestrial laser scanning as an effective tool to retrieve tree level height, crown width, and stem diameter. *Remote Sens.* **2015**, *7*, 1877–1896.
31. Feliciano, E.A.; Wdowinski, S.; Potts, M.D. Assessing mangrove above-ground biomass and structure using terrestrial laser scanning: A case study in the Everglades National Park. *Wetlands* **2014**, *34*, doi:10.1007/s13157-014-0558-6.

32. Othmani, A.; Voon, L. F. L.; Stolz, C.; Piboule A. Single tree species classification from Terrestrial Laser Scanning data for forest inventory. *Pattern Recogn. Lett.* **2013**, *34*, 2144–2150.
33. Kretschmer, U.; Kirchner, N.; Morhart C.; Spiecker, H. A new approach to assessing tree stem quality characteristics using terrestrial laser scans. *Silva Fenn.* **2013**, *47*, id 1071, .
34. Kankare, V.; Joensuu, M.; Vauhkonen, M.; Holopainen, M.; Tanhuanpää, T.; Vastaranta M.; Hyyppä, J.; Hyyppä, H.; Alho, P.; Rikala, J.; *et al.* Estimation of the timber quality of sots pine with terrestrial laser scanning. *EEE Trans. Geosci. Remote Sens.* **2014**, *5*, 1879–1895.
35. Béland, M.; Baldocchi, D.D.; Widlowski, J.-L.; Fournier, R. A.; Verstraete, M.M. On seeing the wood from the leaves and the role of voxel size in determining leaf area distribution of forests with terrestrial LiDAR. *Agric. For. Meteorol.* **2014**, *184*, 82–97.
36. Béland, M.; Widlowski, J.-L.; Fournier, R A. A model for deriving voxel-level tree leaf area density estimates from ground-based LiDAR. *Environ. Modell. Softw.* **2014**, *51*, 184–189.
37. Vonderach, C.; Voegtle, T.; Adler, P. Voxel-based approach for estimating urban tree volume from terrestrial laser scanning data. *Int. Arch. Photogr. Remote Sens. Spat. Inf. Sci.* **2012**, *39*, 451–456.
38. Hess, C.; Bienert, A.; Härdtle, W.; von Oheimb, G. Does tree architectural complexity influence the accuracy of wood volume estimates of single young trees by terrestrial laser scanning? *Forests* **2015**, *6*, 3847–3867.
39. Gorte, B.; Pfeifer, N. Structuring laser-scanned trees using 3D mathematical morphology. *Int. Arch. Photogramm. Remote Sens. Inte* **2004**, *35*, 929–933.
40. Wang, Z.; Zhang, L.; Fang, T.; Mathiopoulos, P.T.; Qu, H.; Chen, D.; Wang, Y. A structure-aware global optimization method for reconstructing 3-D tree models from terrestrial laser scanning data. *Forests* **2014**, *52*, 5653–5669.
41. Dijkstra, E.W. A note on two problems in connexion with graphs. *Numer. Math.* **1959**, *1*, 269–271.
42. Côté, J.F.; Fournier, R.A.; Egli, R. An architectural model of trees to estimate forest structural attributes using terrestrial LiDAR. *Environ. Model. Softw.* **2011**, *26*, 761–777.
43. Shinozaki, K.; Yoda, K.; Hozumi, K; Kria, T. A quantitative analysis of plant form-the pipe model theory: I. Basic analyses. *Jpn. J. Ecol.* **1964**, *14*, 97–105.
44. Côté, J.-F.; Fournier, R.; Frazer, G.; Niemann, K. A fine-scale architectural model of trees to enhance LiDAR-derived measurements of forest canopy structure. *Agric. For. Meteorol.* **2012**, *166*, 72–85.
45. Eysn, L.; Pfeifer, N.; Ressl, C.; Hollaus, M.; Grafl, A.; Morsdorf, F. A practical approach for extracting tree models in forest environments based on equirectangular projections of terrestrial laser scans. *Remote Sens.* **2013**, *5*, 5424–5448.
46. Homepage of the AutoCAD software. Available online: http://autocad.en.softonic.com/ (accessed on 13th November 2015).
47. Belton, D.; Moncrieff, S.; Chapman, J. Processing Tree Point Clouds Using Gaussian Mixture Models. In Proceedings of the ISPRS annals of the photogrammetry, remote sensing and spatial information sciences Antalya, Turkey, 11–13 November 2013; Volume II-5/W2, pp. 43–48.
48. Reynolds, D. Gaussian Mixture Models. *Encyclopedia of Biometrics*; Springer US 2009; pp. 659–663.

49. Raumonen, P.; Kaasalainen, M.; Åkerblom, M.; Kaasalainen, S.; Kaartinen, H.; Vastaranta, M.; Holopainen, M.; Disney, M.; Lewis, P. Fast automatic precision tree models from terrestrial laser scanner data. *Remote Sens.* **2013**, *5*, 491–520.
50. Åkerblom, M.; Raumonen, P.; Kaasalainen, M.; Casella, E. Analysis of geometric primitives in Quantitative Structure Models of Tree Stems. *Remote Sens.* **2015**, *7*, 2072–4292.
51. Bucksch, A.; Lindenbergh, R. CAMPINO—A skeletonization method for point cloud processing. *ISPRS J. Photogramm. Remote Sens.* **2008**, *63*, 115–127. Theme Issue: Terrestrial Laser Scanning.
52. Bucksch, A.; Lindenbergh, R.; Menenti, M. SkelTre. *Vis. Comput.* **2010**, *26*, 1283–1300.
53. Bucksch, A. Revealing the Skeleton from Imperfect Point Clouds. Ph.D. Thesis, Delft University of Technology, Delft, The Netherlands, 2011.
54. Bayer, D.; Seifert, S.; Pretzsch, H. Structural crown properties of Norway spruce (*Picea abies* [L.] Karst.) and European beech (*Fagus sylvatica* [L.]) in mixed versus pure stands revealed by terrestrial laser scanning. *Trees* **2013**, *27*, 1035–1047.
55. Edelsbrunner, H.; Mücke, E.P. Three-dimensional Alpha Shapes. *ACM Trans. Graph.* **1994**, *13*, 43–72.
56. Schilling, A.; Maas, H. Automatic reconstruction of skeletal structures from TLS forest scenes. *ISPRS Ann. Photogramm. Remote Sens. Spatial Inf. Sci.* **2014**, *1*, 321–328.
57. Delagrange, S. ; Jauvin, C. and Rochon, P. PypeTree: A tool for reconstructing tree perennial tissues from point clouds. *Sensors* **2014**, *14*, 4271–4289.
58. Verroust, A.; Lazarus, F. Extracting skeletal curves from 3D scattered data. *Vis. Comp.* **2000**, *16*, 15–25.
59. Runions, A.; Lane, B.; Prusinkiewicz, P. Modeling trees with a space colonization algorithm. *EGWNP* **2007**, *7*, 63–70.
60. Palubicki, W.; Horel, K.; Longay S.; Runions, A.; Lane, B.; Měch, R.; Prusinkiewicz, P. Self-organizing tree models for image synthesis. *ACM Trans. Graph.* **2009**, *58*, 1–10.
61. Stava, O.; Pirk, S.; Kratt, J.; Chen, B.; Měch, R.; Deussen, O.; Benes, B. Inverse procedural modelling of trees. *Comput. Graph. Forum* **2014**, *33*, 118–131.
62. Xu, L.; Mould, D. Procedural tree modeling with guiding vectors. *Comput. Graph. Forum* **2015**, *34*, 47–56.
63. Preuksakarn, C. Reconstructing Plant Architecture from 3D Laser Scanner Data. Ph.D. Thesis, University Montpellier, Montpellier, France, 2012.
64. Xu, H.; Gossett, N.; Chen, B. Knowledge and heuristic-based modeling of laser-scanned trees. *ACM T. Graphic. (TOG)* **2007**, *26*, doi:10.1145/1289603.1289610.
65. Livny, Y.; Yan, F.; Olson, M.; Chen, B.; Zhang, H.; El-Sana, J. Automatic reconstruction of tree skeletal structures from point Clouds. *ACM T. Graphic. (TOG)* **2010**, *29*, 151.
66. Jayaratna, S. Baumrekonstruktion aus 3D-Punktwolken. Diploma Thesis, Institut fur Informatik, Rheinische Friedrich-Wilhelms-Universität, Bonn, Germany, 2009.
67. Yan, D.M.; Wintz, J.; Mourrain, B.; Wang, W.; Boudon, F.; Godin, C. Efficient and robust reconstruction of botanical branching structure from laser scanned points. In Proceedings of the 11th IEEE International Conference on Computer-Aided Design and Computer Graphics, Huangshan, China, 19–21 August 2009; pp. 572–575.

68. Cohen-Steiner, D.; Alliez, P.; Desbrun, M. Variational shape approximation. *ACM Trans. Graph.* **2004**, *23*, 905–914.
69. Aiteanu, F.; Klein, R. Hybrid tree reconstruction from inhomogeneous point clouds. *Vis. Comput.* **2014**, *30*, 763–771.
70. Computree Project. Available online: http://computree.onf.fr/?lang=en (accessed on 17 August 2015).
71. Othmani, A.; Piboule, A.; Krebs, M.; Stolz, C.; Voon, L.L.Y. Towards automated and operational forest inventories with T-Lidar. In Proceedings of 11th International Conference on LiDAR Applications for Assessing Forest Ecosystems (2011 SilviLaser) , Hobart, Australia, 16–19 October 2011.
72. Ravaglia, J.; Alexandra, B.; Piboule, A. Laser-Scanned Tree Stem Filtering for Forest Inventories Measurements. In Proceedings of the Digital Heritage International Congress (DigitalHeritage) Marseille, France, 28 October–1 November 2013, Volume 1, pp. 649–652.
73. Homepage of the Computational Geometry Algorithms Library. Available online: http://www.cgal.org/ (accessed on 24th June 2015).
74. Rusu, R.B.; Cousins, S. 3D is here: Point Cloud Library (PCL). In Proceedings of the IEEE International Conference on Robotics and Automation (ICRA), Shanghai, China, 9–13 May 2011.
75. Homepage of Sorted Publse Data Software Library. Available online: http://www.spdlib.org/doku.php (accessed on 24 June 2015).
76. SimpleTree Project. Available online: http://www.simpletree.uni-freiburg.de/ (accessed on 27 August 2015).
77. SimpleTree Source Code on GitHub. Available online: https://github.com/SimpleTree/SimpleTree (accessed on 26 August 2015).
78. Berkeley Software Distribution. Available online: http://opensource.org/licenses/bsd-license.php (accessed on 26 August 2015).
79. Guennebaud, G.; Jacob, B. Eigen v3, 2010. Available online: http://eigen.tuxfamily.org (accessed on 3 June 2015).
80. Muja, M.; Lowe, D.G. Fast Approximate Nearest Neighbors with Automatic Algorithm Configuration. In Proceedings of the VISAPP International Conference on Computer Vision Theory and Applications, 5–8 February 2009; Insticc, Lisboa, Portugal, 2009, Volume 2.
81. Schroeder, W.; Martin, K.; Lorensen, B. *The Visualization Toolkit: An Object-Oriented Approach to 3D Graphics*, 4th ed.; Kitware: 2004.
82. QT Framework. Available online: http://www.qt.io/ (accessed on 03 June 2015).
83. Rusu, R.B.; Marton, Z.C. ; Blodow, N.; Dolha, M.; Beetz, M. Towards 3D point cloud based object maps for household environments. *Robot. Auton. Syst.* **2008**, *56*, 927–941.
84. Ester, M.; Kriegel, H.P.; Sander, J.; Xu, X. A Density-Based Algorithm for Discovering Clusters in Large Spatial Databases with Noise. In Proceedings of the Second International Conference on Knowledge Discovery and Data Mining, Portland, OR, USA, 2–4 August 1996; pp. 226–231.
85. Fischler, M.A.; Bolles, R.C. Random sample consensus: A paradigm for model fitting with applications to image analysis and automated cartography. *Commun. ACM* **1981**, *24*, 381–395.

86. Olofsson, K. ; Holmgren, J.; Olsson, H. Tree stem and height measurements using terrestrial laser scanning and the RANSAC algorithm. *Remote Sens.* **2014**, *6*, 4323–4344.
87. Spiess, A.-N.; Neumeyer, N. An evaluation of R2 as an inadequate measure for nonlinear models in pharmacological and biochemical research: A Monte Carlo approach. *BMC Pharmacol.* **2010**, 6, *10*.
88. De Berg, M.; van Kreveld, M.; Overmars, M.; Schwarzkopf, O.C. *Computational Geometry*; Springer Berlin Heidelberg, Germany, 2000.
89. Besl, P.J.; McKay, N.D. Method for registration of 3-D shapes. *IEEE Trans. Pattern Anal. Mach. Intell.* **1992**, *14*, 239–256.
90. Creative Commons Non Commercial Share Alike 4.0. Available online: https://creativecommons.org/licenses/by-nc-sa/4.0/ (accessed on 26 August 2015).
91. Wassenberg, M.; Chiu, H.-S.; Guo, W.; Spiecker, H. Analysis of wood density profiles of tree stems: Incorporating vertical variations to optimize wood sampling strategies for density and biomass estimations. *Trees* **2015**, *29*, 551–561.
92. Data Sheet Z + F IMAGER 5010c. Available online: http://www.zf-laser.com/fileadmin/editor/Datenblaetter/Datenblatt_Z_F_IMAGER_5010C_D_kompr.pdf (accessed on 11 June 2015).
93. Data Sheet Z + F IMAGER 5010. Available online: http://www.zf-laser.com/fileadmin/editor/Datenblaetter/Datasheet_Z_F_IMAGER_5010_E_kompr_01.pdf (accessed on 11 June 2015).
94. Temesgen, H.; Affleck, D.; Poudel, K.; Gray, A.; Sessions, J. A review of the challenges and opportunities in estimating above ground forest biomass using tree-level models. *Scand. J. For. Res.* **2015**, *30*, 326–335.
95. Akaike, H. A new look at the statistical model identification. *IEEE Trans. Autom. Control* **1974**, *19*, 716–723, doi:10.1109/TAC.1974.1100705 .
96. Blanchette, D.; Fournier, R.A.; Luther, J.E.; Côté, J.F. Predicting wood fiber attributes using local-scale metrics from terrestrial LiDAR data: A case study of Newfoundland conifer species. *For. Ecol. Manag.* **2015**, *347*, 116–129.
97. Sheppard, J.; Morhart, C.; Hackenberg, J.; Spiecker, H. Terrestrial laser scanning as a tool for assessing tree growth. *Remote Sens.* **2015**, *7*, 1877–1896 .
98. Nelder, B. J.; Mead, R. A simplex method for function minimization. *Comput. J.* **1965**, *4*, 308–313.
99. Press, W. ; Flannery, B. ; Teukolsky, S.; Vetterling, W. *Numerical Recipes 3rd Edition: The Art of Scientific Computing*, 3rd ed.; Cambridge University Press: Cambridge, UK, 2007.
100. Scipy library. Available online: http://docs.scipy.org/doc/ (accessed on 24 June 2015).
101. Breiman, L. Random forests. *Mach. learn.* **2001**,*45*, 5–32.